IEEE Access
Multidisciplinary | Rapid Review | Open Access Journal

Received 19 April 2024, accepted 13 May 2024, date of publication 20 May 2024, date of current version 29 May 2024.

Digital Object Identifier 10.1109/ACCESS.2024.3403486

RESEARCH ARTICLE

Analyzing the Impact of TXOP Allocation on Legacy Devices in IEEE 802.11bd Networks

FARZANEH ABDOLAHI, (Graduate Student Member, IEEE), JELENA MIŠIĆ, (Fellow, IEEE), AND VOJISLAV B. MIŠIĆ, (Senior Member, IEEE)

Department of Computer Science, Toronto Metropolitan University, Toronto, ON M5B 2K3, Canada

Corresponding author: Vojislav B. Mišić (vmisic@torontomu.ca)

The work of Jelena Mišić and Vojislav B. Mišić was supported by the Natural Sciences and Engineering Research Council (NSERC) of Canada through their respective Discovery Grants–Individual.

ABSTRACT This paper presents a comprehensive analysis of V2X communication, focusing on the transition from IEEE 802.11p to IEEE 802.11bd standards, and introduces an analytical framework combining M/G/1 queuing analysis and Markov chain analysis. Our model includes saturation and non-saturation states of Enhanced Distributed Channel Access (EDCA) in the scenarios with and without fallback mechanism for IEEE 802.11bd Next Generation Vehicles (NGV) and focuses on optimizing Transmission Opportunity (TXOP) allocation for legacy (non-NGV) devices whilst taking into account the impact of vehicle-to-roadside Unit (RSU) distance. Our results show increased throughput for higher-priority traffic classes with augmented TXOP allocation for NGV devices and highlight the need to align RSU transmission coverage with On-Board Unit (OBU) data patterns and vehicle distance to prevent network saturation.

INDEX TERMS IEEE 802.11bd, legacy devices, transmission opportunity (TXOP), performance evaluation.

I. INTRODUCTION

In the ever-evolving landscape of vehicular communication, the advent of Vehicle-to-Everything (V2X) technology stands as a pivotal milestone, promising to redefine the dynamics of road safety, traffic efficiency, and the future of transportation. At the core of this evolution are the IEEE 802.11 standards, which have played a crucial role in shaping the communication protocols for both legacy and next-generation vehicles.

The IEEE 802.11p standard, a precursor to the modern V2X ecosystem, laid the groundwork for Dedicated Short-Range Communication (DSRC) [6], offering a communication framework designed to cater to both vehicle-to-vehicle (V2V) and vehicle-to-infrastructure (V2I) communication [15], [17].

However, the landscape of vehicular communication is rapidly advancing, and the arrival of IEEE 802.11bd heralds a new era. Tailored to meet the stringent requirements of NGVs, IEEE 802.11bd is positioned as the next frontier in V2X communication. Its enhancements go beyond the capabilities of IEEE 802.11p, offering improved reliability, reduced latency, and advanced features crucial for the realization of autonomous driving and intelligent transportation systems [7], [14], [19], [21], [30].

Coexistence of NGV and non-NGV devices is achieved by the channel bonding feature of the IEEE 802.11bd MAC layer which allows joint or individual use of two adjacent 10MHz channels, known as the primary and secondary channels. NGV devices can utilize both channels simultaneously, or opt for the primary channel exclusively in the so-called fallback mode, while legacy (non-NGV) stations operate on the secondary channel only.

The cohabitation of legacy devices and their more sophisticated counterparts needs to ensure equitable access, maintain compatibility, and leverage the enhanced capabilities of NGV devices for overall network efficiency. One of the crucial aspects of the coexistence of legacy and next-generation vehicles is the Transmission Opportunity (TXOP) allocation mechanism. Managing TXOP allocation is important to ensure efficient and fair use of the wireless medium while ensuring that both types of devices can coexist seamlessly.

Through the TXOP allocation, a station can request and receive an extended transmission opportunity. Once granted, the station can transmit multiple frames without contending

The associate editor coordinating the review of this manuscript and approving it for publication was Angelo Trotta.

for each frame during the allotted period. It's important to note that the TXOP comes with a predetermined time limit, requiring the station to complete its transmission within this timeframe; otherwise, the station must re-enter the contention process. In this manner, it facilitates prioritization of various types of traffic and offers a number of advantages in a coexistence environment. Firstly, it ensures fair resource allocation by equitably distributing transmission opportunities among different device types, preventing channel monopolization, and promoting balanced resource usage. Secondly, it optimizes airtime utilization which particularly benefits legacy devices with less efficient communication protocols, by minimizing idle time and contention. Thirdly, TXOP sharing facilitates interference mitigation by coordinating transmissions between devices operating on different frequency bands or employing diverse modulation schemes. Additionally, it enables dynamic adaptation to changing network conditions and varying traffic patterns among legacy devices, optimizing resource allocation accordingly.

As the result, TXOP sharing enhances overall throughput and reduces latency, especially in scenarios where NGV devices demand higher data rates or low-latency communication. It also ensures compatibility support for legacy devices, promoting coexistence without extensive modifications. Moreover, coordinating TXOPs contributes to improved reliability by mitigating interference and contention issues faced by legacy devices. Finally, TXOP sharing serves as a migration path for legacy devices towards advanced technologies, facilitating a gradual transition while ensuring coexistence as the network evolves.

In this paper, we evaluate the performance of V2X communication in a coexistence environment that covers both the saturation and non-saturation states of EDCA while accounting for TXOP values, data rates, and arrival rates. It also accounts for different transmission ranges of NGV and legacy devices. It considers scenarios with and without fallback, offering valuable insights into the interaction among the channel bonding scheme, the number of NGV and non-NGV devices, EDCA parameters, different data rates, and TXOP parameters.

Performance evaluation is performed through an analytical framework that integrates M/G/1 queuing analysis and Markov chain analysis. The main contributions of this work can be succinctly outlined as follows.

- **We develop an extensive analytical model that accurately models the EDCA framework with TXOP allocation for coexisting legacy and NGV devices in the network.**
- **We also examine how the network performance is influenced by the distance between the vehicle and the RSU, taking into account the different transmission range of NGV and legacy devices.**
- **Analysis shows that augmenting TXOP allocation for NGV devices results in a modest increase in throughput for higher-priority traffic classes, while the lower-priority classes in both types of devices demonstrate marginal improvements. This is important to ensure a balanced and fair distribution of transmission opportunities, promoting optimal communication for both NGV and legacy (non-NGV) devices.**

The subsequent sections of this paper follow a structured organization. Section II offers a succinct overview of relevant literature. In Section III, we elaborate on the IEEE 802.11bd features. In Section IV, we introduce a probabilistic model detailing activity on the medium, which is subsequently employed in Section V to derive backoff times. Section VI delineates the queuing model for the node buffer, and Section VII presents the Markov chain model. The outcomes of the performance evaluation from the model are discussed in Section VIII. Finally, Section IX provides a conclusion to the paper and suggests potential directions for future research.

II. RELATED WORK

Several studies have extensively examined major V2X communication standards, such as IEEE 802.11p, LTE-V2X, 5G NR-V2X, and IEEE 802.11bd, across diverse usage scenarios [5], [6], [8], [13], [18], [29]. The primary focus of these investigations has been on the comparative evaluation of these standards, particularly in terms of their Physical Layer (PHY) characteristics, with some attention to their Media Access Control (MAC) layer features. However, majority of these studies used simulation-based methodologies [25]. While those studies provide insights into V2X performance metrics and capabilities, there is a need for further exploration into the practical implications and real-world applicability of these standards, especially in terms of MAC layer features, through a more diversified methodological approach that includes analytical modeling.

IEEE 802.11bd integrates elements from both IEEE 802.11n and 802.11ac standards [10]. This includes the channel bonding feature in which a 20MHz channel can be optionally established by combining two adjacent 10MHz channels, facilitating the coexistence of NGV and non-NGV devices. A comparative analysis based on simulation explored various channel access methods, concluding that channel bonding holds the potential to enhance bandwidth utilization under specific conditions [24]. Notably, the referenced papers concentrated on single-channel access for IEEE 802.11p, employing traditional IEEE 802.11n channel bonding solely through simulation experiments.

In [26], an adaptive algorithm tailored for the selection of a contention window is introduced. This algorithm takes into consideration key factors, including compatibility with channel bonding methods, implementation simplicity, and the imperative to avoid modifications to existing devices. The efficacy of this approach is assessed through simulations, considering diverse traffic types and their respective quality of service requirements. Through this evaluation, the algorithm offers a strategic approach to enhance network performance.

A novel channel scheme, referred to as Distributed Triggered Access (DTA) [4], is explicitly crafted for the transmission of critical safety messages in platooning scenarios. In such scenarios, vehicles closely travel together in a formation, aiming to enhance both efficiency and safety. The efficacy of DTA is scrutinized through two distinct methods: a Markov chain model and simulation-based analysis. The focal point is the analysis of DTA's backoff mechanism in order to evaluate both transmission delay and link reliability.

In [27], a comprehensive design for a multi-layered V2X communication technology is outlined, covering the Physical (PHY), Medium Access Control (MAC), and network layers. Notably, this proposal introduces significant modifications to the MAC layer's operation, notably incorporating the use of CSMA/CA without backoff and making Request-to-Send/Clear-to-Send (RTS/CTS) packets optional. These alterations have a considerable impact on network throughput, particularly under conditions of moderate and high load.

Ensuring fair access to communication mediums is crucial, especially in environments where legacy devices coexist with NGV devices. Balancing accessibility across different technologies is essential to promote inclusivity and prevent any undue advantage or disadvantage based on the type of device used, fostering a fair and equitable communication landscape for all users.

The IEEE 802.11p standard, employing TXOP [3], [9], [12], [20], [23], plays a vital role in fostering fair access to the medium, particularly for legacy devices. Our model helps mitigate contention issues by efficiently managing transmission opportunities in IEEE 802.11bd, ensuring that legacy devices coexisting with newer technologies can access the medium fairly. This promotes a more equitable distribution of resources and enhances the overall reliability of communication within the network, irrespective of the device generation. Both legacy and NGV devices use traffic prioritization afforded by the Enhanced Distributed Channel Access (EDCA) scheme with four priority levels [22].

The manner in which WiFi nodes can improve throughput fairness in both 3GPP and proportional fairness concepts is discussed in [16]. The impact of different energy detection (ED) thresholds on coexistence performance is examined in [11]. Lowering the Wi-Fi ED threshold improves performance for both Wi-Fi and LTE-LAA, challenging the assumption that LTE-LAA/LTE-U is treated as noise by Wi-Fi.

Our initial efforts were focused on creating an analytical model specifically for channel bonding without and with fallback in an IEEE 802.11bd network [1], [2]. We have then extended the model to explicitly tackle the performance evaluation of both legacy and NGV devices within IEEE 802.11bd scenarios. In these scenarios, NGV and legacy lower-priority traffic classes utilize TXOP allocation, with due consideration given to the influence of distance to the RSU. Subsequently, we will elaborate on formulating such a comprehensive analytical model.

III. IEEE 802.11BD FEATURES

The development of the IEEE 802.11bd standard introduces several notable innovations, not the least of which is channel bonding. This technique enables simultaneous data transmission across two adjacent channels, leading to enhanced data rates and a reduction in the percentage of stations experiencing unmet Quality of Service (QoS) requirements, particularly regarding packet loss ratio and frame transmission delay. Within IEEE 802.11bd, stations execute the backoff procedure concurrently across both channels to further optimize performance [25].

In no fallback technique, when two adjacent 10MHz channels are free, the backoff counter decreases. However, if either the primary or secondary channels become occupied during the back-off period, the NGV station pauses the counter until both channels are free again. In a scenario where fallback is enabled, if the secondary channel becomes busy during backoff, the NGV STA can shift to the primary channel if it remains idle. Subsequently, the NGV STA must complete the backoff process on the primary channel before transmitting its packet.

In pursuit of higher speeds and Physical Layer (PHY) rates, IEEE 802.11bd emphasizes factors such as spatial streams, Multiple-Input Multiple-Output (MIMO), and channel width. Orthogonal Frequency Division Multiplexing (OFDM) serves as a fundamental modulation method, employing multiple closely spaced orthogonal subcarriers in parallel to achieve enhanced spectral efficiency. Each subcarrier within the IEEE 802.11p/bd standards undergoes Quadrature Amplitude Modulation (QAM) at reduced symbol rates, promoting efficient data transmission.

IEEE 802.11bd integrates features like higher-rate modulation and coding schemes (MCS), resulting in reduced transmission latency and increased throughput by approximately 40 percent. Additionally, the use of Low-Density Parity-Check (LDPC) codes in the physical layer enhances spectral efficiency compared to Binary Convolutional Codes (BCC) utilized in IEEE 802.11p. Moreover, features such as multiple transmit/receive antennas contribute to throughput enhancement through spatial multiplexing and reliability improvement via spatial diversity.

Furthermore, the inclusion of Dual Carrier Modulation (DCM) mode within Vehicular Ad-Hoc Networks (VANETs) based on IEEE 802.11bd extends safety range capabilities. This standard leverages frequency diversity by transmitting identical symbols across widely separated subcarriers, though this necessitates a doubling of the modulation order to maintain throughput levels.

The IEEE 802.11bd standard addresses key issues observed in IEEE 802.11p, particularly regarding packet loss and bit error rates. It introduces mid-ambles, positioned within frames, to reduce bit error rates and permits channel re-estimation during dissemination, enhancing overall reliability. Furthermore, to mitigate CSMA/CA latency inherent

in 802.11p, 802.11bd adopts a strategy of channel contention allocation across distinct channels, with one designated as the primary contention channel and the other as the extension channel, effectively reducing contention overlap. Unlike the 802.11p standard, which supports multi-channel operations over a single radio via 1609.4, 802.11bd utilizes multiple radios. Additionally, 802.11bd leverages 60GHz mmWave technology, offering significant bandwidth, high speed, compact antennas, and exceptional throughput through a number of Modulation and Coding Schemes (MCS).

IV. PROPOSED SYSTEM MODEL

We consider four traffic categories for both NGV and legacy devices, each with different priorities labeled as $AC_{X,k}$ (where $k = 0, 1, 2, 3$). Our model incorporates the TXOP function, accounting for distance effects on the network, wherein the NGV STAs with four access categories and the non-NGV STAs with lower priority traffic classes can gain control of the medium and transmit multiple frames. TXOP bandwidth is allocated sequentially, frame by frame, until either the node's buffer is emptied or the maximum TXOP allocation limit, denoted as $M_{X,k}$ frames for traffic class k, is reached following a successful backoff.

Incoming packets destined for NGV or non-NGV nodes, categorized by class k, follow a Poisson process with an arrival rate of $\lambda_{X,k}$, where subscript X denotes NGV or non-NGV STA. **Due to differing data rates between non-NGV and NGV STAs, the duration of the MAC Protocol Data Unit (MPDU) for the $ld_{Y,k}[j]$ slot varies, with label Y representing three types of channel access probability (secondary, primary, channel bonding), and the label j indicates the distance of each device from the RSU.** We assume a time slot of $\omega = 13\mu s$ for compatibility with legacy devices. The backoff process is modeled using the queuing model of each node and the Markov chain model.

In this investigation, we focus on the area around a single RSU operating in a non-saturation state, situated along a bidirectional road segment as depicted in Figure 4. The road segment is divided into multiple regions based on the RSU's location, with vehicles in each region having different payload transmission rates depending on their distance from the RSU.

In case of channel collision or noise error, the node initiates a waiting period defined by EIFS, calculated as $AIFSN + ack + 1$ slot, before commencing the backoff process. The probability of no RTS error, denoted as $\delta_{Y,r}$, is computed as $(1 - ber_{Y,k})^{rts}$, while the probability of no CTS error, denoted as $\delta_{Y,c}$, is calculated as $(1 - ber_{Y,k})^{cts}$, both arising from channel noise. The probability that neither RTS nor CTS is affected by channel noise is, then, $\delta_{Y,k} = (1 - ber_{Y,k})^{rts+cts}$. Furthermore, probability that a data transmission is unaffected by channel noise is $\sigma_{Y,k} = (1 - ber_{Y,k})^{l_d \cdot 8 + MACheader + ack}$, with l_d representing the packet size in bytes (MSDU) and $ber_{Y,k}$ denoting the bit error rate in respective channels.

Prior to commencing a backoff countdown for both non-NGV and NGV devices, and after the medium becomes busy throughout the backoff countdown, these stations must wait for a duration defined as $AIFS_{x,k} = SIFS + AIFSN_{x,k} \cdot \omega$, where $AIFSN_{x,k}$ is the number specific to non-NGV and NGV STAs. The initial values for the freezing counters when $k = 0 \ldots 3$ are set as follows: $B_{X,k} = AIFSN_{X,k} - AIFSN_{X,3}$. It should be noted that access via $AIFS_{X,3}$ is not feasible as access is synchronized with the end of the previous dissemination.

The maximum allowable duration for legacy or NGV devices to access the medium is denoted as $A_{X,k,max}$, which can be defined as

$$A_{X,k,max} = \begin{cases} AIFSN_{X,k-1} - AIFSN_{X,k}, & k = 1 \ldots 3 \\ W_{X,0,max}, & k = 0 \end{cases} \quad (1)$$

Within the EDCA framework, a station counts down the backoff counter to zero before each transmission attempt. In the event of a collision, the backoff strategy must be repeated with an increase in the backoff window size $CW_{k,i}$. The backoff counter is initialized with a value uniformly distributed in the range of [0, w]. There are a total of $m_{X,k} + 1$ backoff phases, starting from phase 0. Although the frame can be re-transmitted up to R times, the window size will only expand until it reaches phase $m_{X,k}$. The size of the contention window for access category k in the i-th backoff stage, where i ranges from 0 to $m_{X,k}$, is:

$$W_{X,k,i} = \begin{cases} 2^i W_{X,k,0}, & 0 \le i \le m_{X,k} \\ 2^{m_{X,k}} W_{X,k,0} = W_{X,k,max}, & m_{X,k} < i \le R \end{cases} \quad (2)$$

The probability of each slot being idle for both non-NGV and NGV devices within the $A_{X,k,max}$ period, without fallback, when k ranges from 0 to 3, can be formulated as follows:

$$f_{X,k} = \prod_{i=k}^{3} (1 - \tau_{s,i})^{n_{L,i}} \prod_{j=k}^{3} (1 - \tau_{b,j})^{n_{N,j}} \quad (3)$$

Likewise, the idle probability of IEEE 802.11bd with fallback can be denoted as:

$$\begin{aligned} f_{L,k} &= \prod_{i=k}^{3} (1 - \tau_{s,i})^{n_{L,i}} \prod_{j=k}^{3} (1 - \tau_{b,j})^{n_{N,j}} \\ f_{N,k} &= \prod_{l=k}^{3} (1 - \tau_{p,l})^{n_{N,l}} \prod_{i=k}^{3} (1 - \tau_{s,i})^{n_{L,i}} \prod_{j=k}^{3} (1 - \tau_{b,j})^{n_{N,j}} \end{aligned} \quad (4)$$

In the above equations, the transmission probability for non-NGV devices is represented by τ_s, while for NGV devices, it is denoted by τ_b for the wide channel and τ_p for the primary channel. Additionally, $n_{X,k}$ refers to the number of legacy and NGV devices in each access category.

In the absence of fallback, the reduction of the backoff counter for $AC_{X,0}$ occurs within $A_{X,0,max}$ if the time slot remains inactive during this period. Consequently, the

associated probability of backoff counter decrement is $\frac{f_{X,0}}{1-\tau_{Y,0}}$, where the label Y is employed for both types of channel access probability. The denominator takes into account the situation where other ACs are not transmitting when $AC_{X,0}$ is in the backoff state. For $AC_{X,1}$, the backoff counter can decrease if the medium is idle during both $A_{X,0,max}$ and $A_{X,1,max}$. When $AC_{X,1}$ is in the backoff state, the probabilities of a time slot being idle during the $A_{X,1,max}$ and $A_{X,0,max}$ periods are $\frac{f_{X,1}}{1-\tau_{Y,1}}$ and $\frac{f_{X,0}}{1-\tau_{Y,1}}$, respectively. The normalized probability of backoff counter decrement for $AC_{X,1}$ is determined during these two periods by combining the probabilities of idle time slots with the overall probability of the $A_{X,1,max}$ period being idle. The probability of backoff counter decrement in the scenario without fallback for non-NGV and NGV STAs can be articulated as:

$$g_{X,k} = \begin{cases} \dfrac{f_{X,0}}{1-\tau_{Y,0}}, & k = 0 \\ (1-f_{X,k}^{A_{X,k,max}})\dfrac{f_{X,k}}{1-\tau_{Y,k}} & \\ \quad +f_{X,k}^{A_{X,k,max}} g_{X,k-1}\dfrac{1-\tau_{Y,k-1}}{1-\tau_{Y,k}}, & k = 1,2,3 \end{cases} \tag{5}$$

In the context of 802.11bd channel bonding with fallback, if the secondary channel becomes occupied during the backoff operation while the primary channel stays unoccupied, NGV devices have the option to switch to the primary single channel and transmit the NGV PPDU on it. This investigation presents models for the NGV channel access probability in both primary and wide channel operations, denoted as τ_p and τ_b, respectively. In this framework, the probability of backoff counter decrement for non-NGV STAs can be expressed as:

$$g_{L,k} = \begin{cases} \dfrac{f_{L,0}}{1-\tau_{s,0}}, & k = 0 \\ (1-f_{L,k}^{A_{L,k,max}})\dfrac{f_{L,k}}{1-\tau_{s,k}} & \\ \quad +f_{L,k}^{A_{L,k,max}} g_{L,k-1}\dfrac{1-\tau_{s,k-1}}{1-\tau_{s,k}}, & k = 1,2,3 \end{cases} \tag{6}$$

while the associated probability for an NGV device is

$$g_{N,k} = \begin{cases} \dfrac{f_{N,0}}{P_{b,0}(1-\tau_{b,0})+Q_{p,0}(1-\tau_{p,0})}, k = 0 \\ (1-f_{N,k}^{A_{N,k,max}})\dfrac{f_{N,k}}{P_{b,k}(1-\tau_{b,k})+Q_{p,k}(1-\tau_{p,k})} & \\ \quad +f_{N,k}^{A_{N,k,max}} g_{N,k-1} & \\ \cdot\dfrac{P_{b,k-1}(1-\tau_{b,k-1})+Q_{p,k-1}(1-\tau_{p,k-1})}{P_{b,k}(1-\tau_{b,k})+Q_{p,k}(1-\tau_{p,k})}, k = 1,2,3 \end{cases} \tag{7}$$

In the provided equations, $g_{X,k}$ denotes the probability that only one $AC_{X,k}$ accesses the medium during a slot, which is equivalent to the probability that a $AC_{X,k}$ transmission avoids collisions. **Here, $\gamma_{X,k}$ represents the probability of non-collision during transmission, defined as $\gamma_{X,k} = g_{X,k}$ for k ranging from 0 to 3.** Additionally, P and Q represent the access probabilities to the wide channel and primary channel, respectively, and these probabilities can be computed as:

$$\begin{aligned} P_{b,0} &= (1-\tau_{b,0})^{n_{N,0}-1}(1-\tau_{p,0})^{n_{N,0}-1} \\ &\quad \cdot\prod_{i=0}^{3}(1-\tau_{s,i})^{n_{L,i}}\prod_{l=1}^{3}(1-\tau_{b,l})^{n_{N,l}}\prod_{j=1}^{3}(1-\tau_{p,j})^{n_{N,j}} \\ Q_{p,0} &= 1-P_{b,0} \\ P_{b,1} &= (1-\tau_{b,1})^{n_{N,1}-1}(1-\tau_{p,1})^{n_{N,1}-1} \\ &\quad \cdot\prod_{i=0}^{3}(1-\tau_{s,i})^{n_{L,i}}\prod_{l=2}^{3}(1-\tau_{b,l})^{n_{N,l}}\prod_{j=2}^{3}(1-\tau_{p,j})^{n_{N,j}} \\ Q_{p,1} &= 1-P_{b,1} \\ P_{b,2} &= (1-\tau_{b,2})^{n_{N,2}-1}(1-\tau_{p,2})^{n_{N,2}-1} \\ &\quad \cdot\prod_{i=0}^{3}(1-\tau_{s,i})^{n_{L,i}}(1-\tau_{b,3})^{n_{N,3}}(1-\tau_{p,3})^{n_{N,3}} \\ Q_{p,2} &= 1-P_{b,2} \\ P_{b,3} &= (1-\tau_{b,3})^{n_{N,3}-1}(1-\tau_{p,3})^{n_{N,3}-1}\prod_{i=0}^{3}(1-\tau_{s,i})^{n_{L,i}} \\ Q_{p,3} &= 1-P_{b,3} \end{aligned} \tag{8}$$

V. MODELING THE BACKOFF PROCEDURE

We utilized a Discrete Time Markov Chain (DTMC) to depict the backoff process in our model. This model integrates two counters, namely the backoff counter (j) and the freezing counter ($B_{x,k}$), assigned to each state of the chain and a specific backoff phase. The probability $P_{X,eifs,k}$, where k = 0 . . 3, signifies the probability of an EIFS event occurring for both non-NGV and NGV devices, and its calculation is expressed as:

$$P_{X,eifs,k} = 1-\gamma_{X,k}\delta_{Y,k}\sigma_{Y,k}. \tag{9}$$

Figure 1 illustrates the fundamental component of the Markov chain model, showcasing the freezing countdown process's behavior for both non-NGV and NGV devices during the backoff phase, i. It's important to emphasize that the value of $AIFSN_{X,k}$ in the IEEE 802.11bd amendment remains consistent with that of IEEE 802.11p. However, the number of states and conditions for state transitions in the freezing counter differ in the amendment.

The vertical input probability, In1, and the lateral input probability, In2, act as external inputs for each block. In1 is derived from the preceding backoff phase (i-1), while In2 originates from the previous backoff state (j-1) within the same backoff phase (i). Notably, In2 is set to zero when the value of the backoff counter, $j = W_{k,i} - 1$.

The freezing block in both Legacy and NGV STAs exhibits the cumulative state probabilities for all non-zero backoff

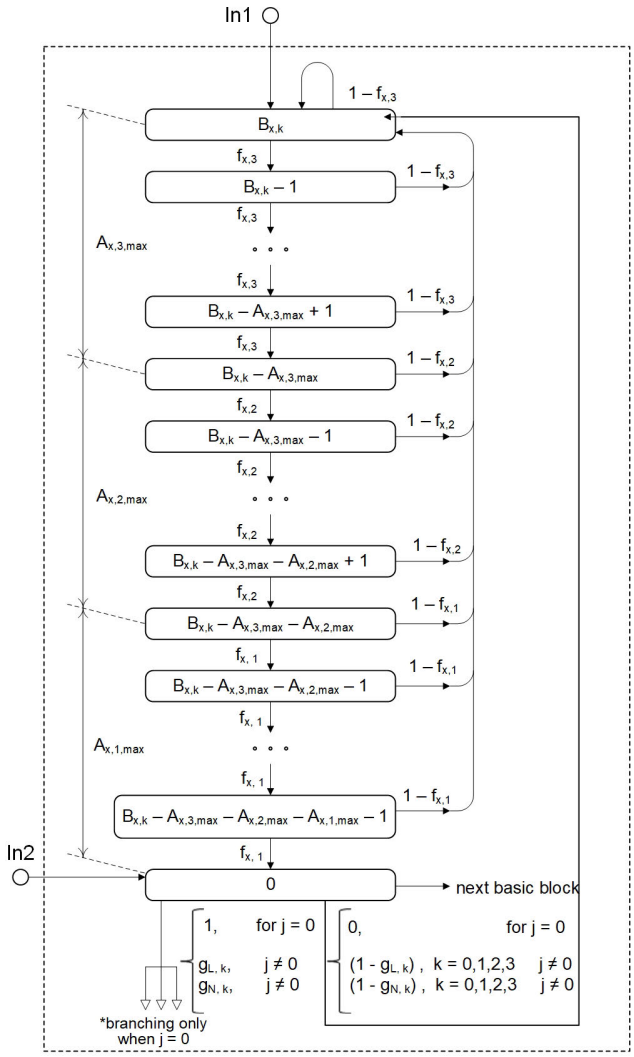

FIGURE 1. Markov chain modeling the backoff process.

counter values as: $P_{X,k} = In_{X,2} + (In_{X,1} + In_{X,2}(1 - g_{X,k}))Fl_{X,k}, k = 0..3$. When $k < 3$, the value of $Fl_{X,k}$ is

$$Fl_{X,k} = \frac{1}{g_{X,k}} \left(1 + \frac{\sum_{i=k+1}^{3} \sum_{n=0}^{A_{X,i,max}-1} f_{X,i}^{n} \prod_{l=i+1}^{3} f_{X,l}^{A_{X,l,max}}}{\prod_{i=k+1}^{3} f_{X,i}^{A_{X,i,max}}} \right) \quad (10)$$

where $Fl_{X,3} = \frac{2}{g_{X,3}}$. If, in a product operation, the lower limit surpasses the upper limit, the product operator results in 1. In the freezing counter block for both legacy and NGV devices, when the backoff counter value is zero, there is no loopback from the bottom state to the top state. Consequently, the sum of probabilities in the freezing counter block can be expressed as: $P_{X,k} = In_{X,2} + In_{X,1} g_{X,k} Fl_{X,k}, k = 0..3$.

The Probability Generating Function (PGF) representing the successful packet transmission time in both legacy and NGV devices operating without fallback can be formulated as

$$St_{X_{wo},k} = z^{rts+cts+ld_{Y,k}+3sifs+ack+AIFS_{X,k}+(av\phi_{X,k}+0.5)} \quad (11)$$

while the PGF for the situation where NGV devices operate with fallback is

$$\begin{aligned} St_{L_w,k} &= z^{rts+cts+ld_{s,k}+3sifs+ack+AIFS_{L,k}+(av\phi_{L,k}+0.5)} \\ St_{N_w,k} &= z^{rts+cts+ld_{b,k}+ld_{p,k}+ack+4sifs+AIFS_{N,k}+(av\phi_{N,k}+0.5)} \end{aligned} \quad (12)$$

Here, $av\phi_{x,k}$ denotes the average Probability PGF for the number of packets during the service period with errors.

PGF for unsuccessful bandwidth reservation in legacy and NGV devices can be computed as

$$\begin{aligned} Ct_{X_{wo},k} &= \gamma_{X,k}\delta_{Y,r}(1-\delta_{Y,c})z^{rts+sifs+cts+ld_{Y,k}+3sifs+ack} \\ &\quad + (1-\gamma_{X,k}\delta_{Y,r}(1-\delta_{Y,c}))z^{rts+sifs+cts} \end{aligned} \quad (13)$$

in no fallback case and

$$\begin{aligned} Ct_{L_w,k} &= \gamma_{L,k}\delta_{s,r}(1-\delta_{s,c})z^{rts+sifs+cts+ld_{s,k}+3sifs+ack} \\ &\quad + (1-\gamma_{L,k}\delta_{s,r}(1-\delta_{s,c}))z^{rts+sifs+cts} \\ Ct_{N_w,k} &= \gamma_{N,k}\delta_{Y,r}(1-\delta_{Y,c})z^{rts+sifs+cts+ld_{b,k}+ld_{p,k}+4sifs+ack} \\ &\quad + (1-\gamma_{N,k}\delta_{Y,r}(1-\delta_{Y,c}))z^{rts+sifs+cts} \end{aligned} \quad (14)$$

in a situation where NGV devices operate with fallback.

Please find the other formulas and derivations in the Appendix.

VI. QUEUING MODEL OF A NODE

To comprehensively illustrate the system's potential outcomes after the backoff, transmission, and idle states, it is essential to depict the system with the aid of a timing diagram and a Markov chain, as shown in Figures 2 and 3, respectively. Both visualizations are tailored to a particular traffic class for both types of devices. For each transmission, a maximum of $M_{X,k}$ data frames can be consecutively sent. If an error leads to an unacknowledged data frame, it must be promptly retransmitted after the initial transmission. This retransmission can occur within the same TXOP allocation if there is sufficient available time, or after another backoff attempt if not. It is imperative to identify all time intervals between two consecutive transmission attempts, which include:

- The zeroth backoff phase for class k commences right after the TXOP transmission ends, as illustrated by the time interval marked as $V_{X,0}$ in Figure 2. It's worth noting that the subscript 0 indicates the time index, not the traffic class index. The PGF for this period is represented as $B_{X,k,0}(z)$. To proceed with additional calculations, we require the LST of this time, denoted as $B^*_{X,k,0}(s) = B_{X,k,0}(exp(-s))$. The probability of mass for the arrival of i frames during this period will be represented as $\upsilon^0_{X,k,i}$. The PGF for the number of frame arrivals during this time is $F_{X,k,0}(z) = B^*_{X,k,0}(\lambda_{X,k} - \lambda_{X,k}z) = \sum_{i=1}^{\infty} \upsilon^0_{X,k,i} z^i$.

- The continuation of the backoff process following the zeroth phase occurs when a frame arrives during the zeroth backoff but the transmission attempt is unsuccessful. This specific period is referred to as $V_{X,1}$ in Figure 2. PGF for this time period is $Bzof_{X,k}(z)$ and its LST is $Bzof^*_{X,k}(z) = Bzof_{X,k}(exp(-s))$. $\upsilon^1_{X,k,i}$ is the mass probability for the arrival of i frames during this period. $F_{X,k,1}(z) = Bzof^*_{X,k}(\lambda_{X,k} - \lambda_{X,k}z)$ is PGF for the number of frame arrivals during this period.
- The full backoff phase occurs when the node's buffer is not empty after the TXOP transmission, corresponding to period $V_{X,2}$ in Figure 2. The PGF and LST for this time is $Bof_{X,k}(z)$ and $Bof^*_{X,k}(s) = Bof_{X,k}(exp(-s))$ respectively. $\upsilon^2_{X,k,i}$ is the mass probability for the arrival of i frames during this time. $F_{X,k,2}(z) = Bof^*_{X,k}(\lambda_{X,k} - \lambda_{X,k}z)$ is PGF for the number of frame arrivals during this period.
- The node enters an idle state if there were no frame arrivals during the zeroth backoff, as depicted in the period I in Figure 2. The first arrival during this idle state will terminate it and trigger the initiation of $AIFS_{X,k}$ traversal.
- The time it takes to traverse through the $AIFS_{X,k}$ freezing counter upon exiting the idle state is crucial. This transmission attempt will succeed only if the medium remains idle for $AIFSN_{X,k}$ time slots; otherwise, a complete backoff procedure is required before packet transmission can occur. This specific time period is marked as $V_{X,3}$ in Figure 2, and its LST follows a particular form of $V^*_{X,3}(s) = exp(-s.AIFS_{X,k})$. The mass probability for the arrival of i frames during this period will be indicated as $\upsilon^3_{X,k,i}$. PGF for the number of arrivals during this period is $F_{X,k,3}(z) = V^*_{X,k,3}(\lambda_{X,k} - \lambda_{X,k}z)$.

Modeling the buffer state of the node is essential for both non-NGV and NGV devices at the commencement of the TXOP service and after each frame departs during the TXOP service. The variables $q^+_{X,K,i}$ (where $k = 0..3$ and $i > 0$) and $\pi^{\mu}_{X,k,i}$ (where $\mu = 1..M_{X,K}$) signify the mass probability for having i frames in the buffer at the initiation of the service and following the departure of the μ-th frame, respectively. Referring to Figs. 2 and 3, the expression for the node buffer status at the service's onset can be represented as:

$$q^+_{X,k,i} = \sum_{\mu=1}^{M_{X,k}} \pi^{\mu}_{X,k,0}\upsilon^0_{X,k,0} \cdot \left(f^{aifs_{X,k}}_{X,0}\upsilon^3_{X,k,i-1} + (1 - f^{aifs_{X,k}}_{X,0}) \sum_{j=1}^{i-1} \upsilon^3_{X,k,j}\upsilon^2_{X,k,i-j} \right) + \sum_{\mu=1}^{M_{X,k}} \pi^{\mu}_{X,k,0}\upsilon^0_{X,k,i}\gamma_{X,k}\delta_{Y,k} + \sum_{\mu=1}^{M_{X,k}} \pi^{\mu}_{X,k,0} \sum_{l=1}^{i} \upsilon^0_{X,k,l}(1 - \gamma_{X,k}\delta_{Y,k})\upsilon^1_{X,k,i-l}$$

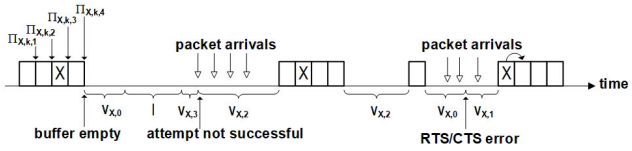

FIGURE 2. Timing diagram for backoff, idle state, and packet servicing for legacy and NGV devices where $M_{X,k} = 4$.

$$+ \sum_{j=1}^{i} \pi^{M_{X,k}}_{X,k,j}\upsilon^2_{X,k,i-j} \tag{15}$$

The right-hand side of the above equation comprises four components. The first component relates to the scenario in which the node transitions to the idle state after the zeroth backoff with no frame arrivals. Exiting this idle state occurs upon the arrival of a frame, leading to two potential outcomes. If the traversal through the freezing counter $AIFS_{X,k}$ is successful, a transmission occurs, and the buffer's content increases by the number of frames arriving during the $AIFS_{X,k}$ countdown. Conversely, an unsuccessful traversal through $AIFS_{X,k}$ prompts the node to initiate a regular backoff phase, augmenting the queue length by the number of frames that arrived during the traversal and the subsequent regular backoff.

The second component considers the increase of the queue length when frames arrived during the zeroth backoff phase, and the first transmission attempt proved successful.

The third component deals with scenarios where frame arrivals occurred during the zeroth backoff phase, but the initial transmission attempt failed, leading to the continuation of the backoff process until a successful transmission was achieved.

The fourth component characterizes the queue length when the buffer remains non-empty after the preceding transmission, requiring the initiation of the regular backoff process.

Also, we derived generating functions (GFs) for the number of frames in the node's queue for both devices at the beginning of the TXOP service and after each frame is transmitted. Specifically: $Q^+_{X,k}(z) = \sum_{i=1}^{\infty} q^+_{X,k,i}z^i$, and $\Pi_{X,k,\mu}(z) = \sum_{i=1}^{\infty} \pi^{\mu}_{X,k,i}z^i$, $\mu = 1..M_{X,k}$.

$$Q^+_{X,k}(z) = \sum_{i=1}^{\infty} z^i \sum_{\mu=1}^{M_{X,k}} \pi^{\mu}_{X,k,0}\upsilon^0_{X,k,0}(f^{aifs_{x,k}}_{X,0}\upsilon^3_{X,k,i-1} + (1 - f^{aifs_{x,k}}_{X,0}) \sum_{j=1}^{i-1} \upsilon^3_{X,k,j}\upsilon^2_{X,k,i-j}) + \sum_{i=1}^{\infty} z^i \sum_{\mu=1}^{M_{X,k}} \pi^{\mu}_{X,k,0}\upsilon^0_{X,k,i}\gamma_{X,k}\delta_{Y,k} + \sum_{i=1}^{\infty} z^i \sum_{\mu=1}^{M_{X,k}} \pi^{\mu}_{X,k,0} \sum_{l=1}^{i} \upsilon^0_{X,k,l}(1 - \gamma_{X,k}\delta_{Y,k})\upsilon^1_{X,k,i-l}$$

$$+\sum_{i=1}^{\infty} z^i \sum_{j=1}^{i} \pi_{X,k,j}^{M_{X,k}} \upsilon_{X,k,i-j}^{2} \tag{16}$$

After summation (potentially involving a change in the order of summation), we have

$$\begin{aligned} Q_{X,k}^{+}(z) = {} & zF_{X,k,3}(z) \sum_{\mu=1}^{M_{X,k}} \pi_{X,k,0}^{\mu} \upsilon_{X,k,0}^{0} \\ & \cdot \left(f_{X,0}^{aifs_{X,k}} \upsilon_{X,k,i-1}^{3} + (1 - f_{X,0}^{aifs_{X,k}}) F_{X,k,2}(z) \right) \\ & + (F_{X,k,0}(z) - \upsilon_{X,k,0}^{0}) \sum_{\mu=1}^{M_{X,k}} \pi_{X,k,0}^{\mu} \\ & \cdot \left(\delta_{Y,k} \gamma_{X,k} + (1 - \delta_{Y,k} \gamma_{X,k}) F_{X,k,1}(z) \right) \\ & + (\Pi_{M_{X,k}}(z) - \pi_{X,k,0}^{M_{X,k}}) F_{X,k,2}(z) \end{aligned} \tag{17}$$

PGF for the number of frame arrivals during the frame service time is formulable for both device types, assuming NGV devices do not employ fallback, in the following manner:

$$A_{X,k} = e^{\lambda_{X,k}(z-1)(ld_{Y,k} + ACK + 3sifs)} \tag{18}$$

Similarly, PGF for the number of frame arrivals during the frame service time for both non-NGV and NGV STAs in the fallback scenario can be expressed as:

$$\begin{aligned} A_{L,k} &= e^{(\lambda_{L,k}(z-1)(ld_{s,k} + ACK + 3sifs))} \\ A_{N,k} &= e^{(\lambda_{N,k}(z-1)(ld_{b,k} + ld_{p,k} + ACK + 4sifs))} \end{aligned} \tag{19}$$

Then, we can write $A_{X,k}(z) = \sum_{i=0}^{\infty} a_{X,k,i} z^i$, where values of $a_{X,k,i}$ denote the mass probability of i frame arrivals during the frame service time. We can similarly express the equation for the number of frames in the buffer after the first departure in the TXOP service period as

$$\begin{aligned} \pi_{X,k,0}^{1} &= q_{X,k,1}^{+} \sigma_{Y,k} a_{X,k,0} \\ \pi_{X,k,i}^{1} &= \sum_{j=1}^{i+1} q_{X,k,j}^{+} \sigma_{Y,k} a_{X,k,i-j+1} \\ &\quad + \sum_{j=1}^{i} q_{X,k,j}^{+} \sigma_{Y,k} a_{X,k,i-j} \end{aligned} \tag{20}$$

$$\begin{aligned} \pi_{X,k,0}^{\mu} &= \pi_{X,k,1}^{\mu-1} \sigma_{Y,k} a_{X,k,0} \\ \pi_{X,k,i}^{\mu} &= \sum_{j=1}^{i+1} \pi_{X,k,j}^{\mu-1} \sigma_{Y,k} a_{X,k,i-j+1} \\ &\quad + \sum_{j=1}^{i} \pi_{X,k,j}^{\mu-1} \sigma_{Y,k} a_{X,k,i-j} \end{aligned} \tag{21}$$

For $i > 0$ (i.e., in the second and fourth equations above), the initial term on the right-hand side corresponds to the scenario in which frame transmission was successful and frame leaves the buffer, while the second term pertains to the case where frame transmission was unsuccessful.

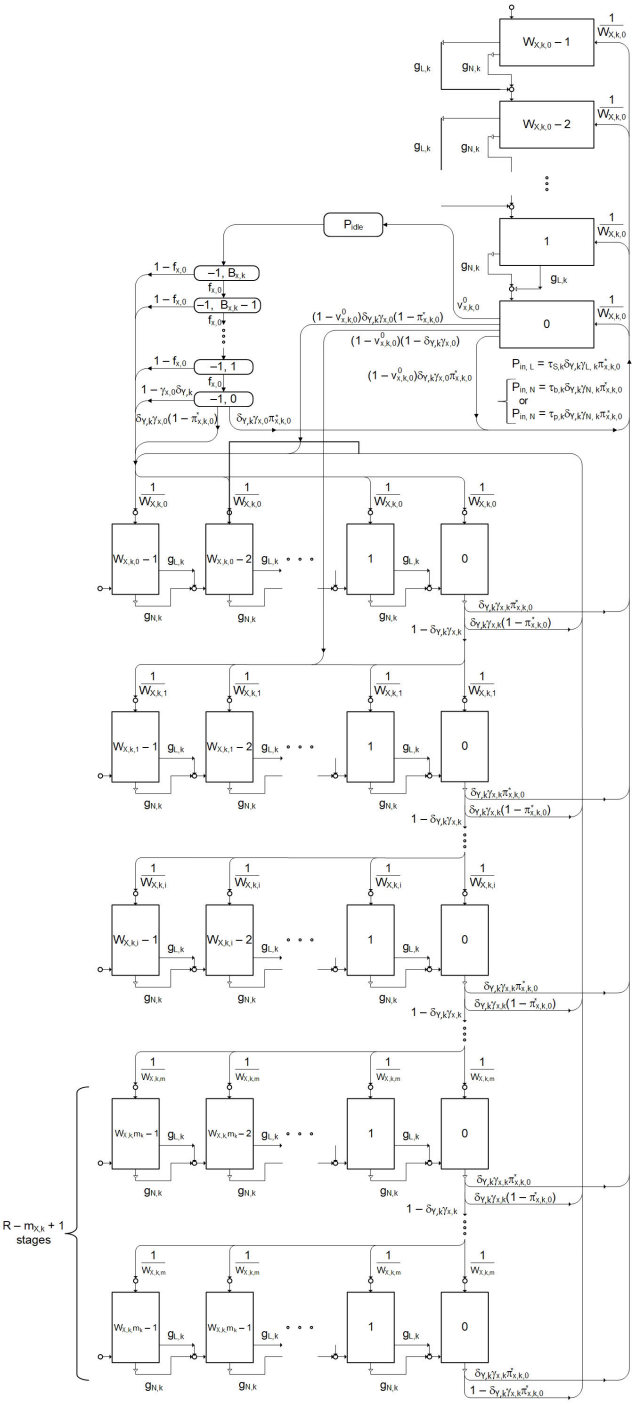

FIGURE 3. Markov chain model for non-NGV and NGV devices.

The generating function (GF) for the number of frames in the buffer after each frame is transmitted is

$$\begin{aligned} \Pi_{X,k,1}(z) = {} & \sum_{i=0}^{\infty} z^i \sum_{j=1}^{i+1} q_{X,k,j}^{+} \sigma a_{X,k,i-j+1} \\ & + \sum_{i=1}^{\infty} z^i \sum_{j=1}^{i} q_{X,k,j}^{+} \sigma_{Y,k} a_{X,k,i-j} \end{aligned} \tag{22}$$

Upon summation, we derive:

$$\begin{aligned}\Pi_{X,k,1}(z) &= \frac{\sigma_{Y,k}A_{X,k}(z)}{z}Q^{+}_{X,k}(z) \\ &\quad + (1-\sigma_{Y,k})A_{X,k}(z)Q^{+}_{X,k}(z) \\ &= Q^{+}_{X,k}(z)\frac{A_{X,k}(z)errfr(z)}{z}\end{aligned} \tag{23}$$

where $errfr(z) = \sigma + (1-\sigma)z$ and σ represents the PGF for the increment in the frame number within the queue due to a transmission error.

The PGF for the disparity between the number of frame arrivals and departures during the service of a single frame can be articulated as

$$\Omega_{X,k}(z) = \frac{A_{X,k}(z)errfr(z)}{z} \tag{24}$$

and then we get

$$\Pi_{X,k,\mu}(z) = (\Pi_{X,k,\mu-1}(z) - \pi^{\mu-1}_{X,k,0})\Omega_{X,k}(z) \tag{25}$$

$Q^{+}_{X,k}(z)$ and $\Pi_{X,k,\mu}(z)$ are not proper PGFs as they do not equal 1. These are GFs incorporating mass probability distributions for the queue length at a specific observation point within the system. However, the sum of probabilities of system states at the initiation of service and after each transmission must add up to one. Therefore, it follows that $Q^{+}_{X,k}(1) + \sum_{\mu=1}^{M_{X,k}} \Pi_{X,k,\mu}(1)$ equals 1. To address this, it is necessary to express all GFs of $\Pi_{X,k,\mu}(z)$ as functions of $Q^{+}_{X,k}(z)$:

$$\begin{aligned}\Pi_{X,k,2}(z) &= Q^{+}_{X,k}(z)\Omega_{X,k}(z)^2 - \pi^{1}_{X,k,0}\Omega_{X,k}(z) \\ \Pi_{X,k,3}(z) &= Q^{+}_{X,k}(z)\Omega_{X,k}(z)^3 - \pi^{1}_{X,k,0}\Omega_{X,k}(z)^2 \\ &\quad - \pi^{2}_{X,k,0}\Omega_{X,k}(z) \\ &\quad \cdots \\ \Pi_{X,k,\mu}(z) &= Q^{+}_{X,k}(z)\Omega_{X,k}(z)^{\mu} - \sum_{j=1}^{\mu-1}\pi^{j}_{X,k,0}\Omega_{X,k}(z)^{\mu-j}\end{aligned} \tag{26}$$

So we can obtain

$$\begin{aligned}&Q^{+}_{X,k}(z) \\ &= \frac{zF_{X,k,3}(z)\upsilon^{0}_{X,k,0}\sum_{\mu=1}^{M_{X,k}}\pi^{\mu}_{X,k,0}}{1-F_{X,k,2}(z)\Omega_{X,k}(z)^{M_{X,k}}} \\ &\frac{(\sigma_{Y,k}f^{aifs_{x,k}}_{X,0} + (1-\sigma_{Y,k}f^{aifs_{x,k}}_{X,0})F_{X,k,2}(z))}{1-F_{X,k,2}(z)\Omega_{X,k}(z)^{M_{X,k}}} \\ &+ \frac{(F_{X,k,0}(z)-\upsilon^{0}_{X,k,0})\sum_{\mu=1}^{M_{X,k}}\pi^{\mu}_{X,k,0}[\delta_{Y,k}\gamma_{X,k} + F_{X,k,1}(z)}{1-F_{X,k,2}(z)\Omega_{X,k}(z)^{M_{X,k}}} \\ &\frac{(1-\delta_{Y,k}\gamma_{X,k})] - F_{X,k,2}(z)\sum_{j=1}^{M_{X,k}}\pi^{j}_{X,k,0}\Omega_{X,k}(z)^{M_{X,k}-j}}{1-F_{X,k,2}(z)\Omega_{X,k}(z)^{M_{X,k}}}\end{aligned} \tag{27}$$

After multiplying both the numerator and denominator by $z^{M_{X,k}}$, we obtain:

$$\begin{aligned}Q^{+}_{X,k}(z) &= \frac{z^{M_{X,k}+1}F_{X,k,3}(z)\upsilon^{0}_{X,k,0}}{z^{M_{X,k}} - F_{X,k,2}(z)(z\Omega_{X,k}(z))^{M_{X,k}}} \\ &\quad \cdot \sum_{\mu=1}^{M_{X,k}}\pi^{\mu}_{X,k,0}(\sigma_{Y,k}f^{aifs_{X,k}}_{X,0} + (1-\sigma_{Y,k}f^{aifs_{X,k}}_{X,0})F_{X,k,2}(z)) \\ &\quad + \frac{z^{M_{X,k}}(F_{X,k,0}(z)-\upsilon^{0}_{X,k,0})}{z^{M_{X,k}} - F_{X,k,2}(z)(z\Omega_{X,k}(z))^{M_{X,k}}} \\ &\quad \cdot \sum_{\mu=1}^{M_{X,k}}\pi^{\mu}_{X,k,0}[\delta_{Y,k}\gamma_{X,k} + F_{X,k,1}(z)(1-\delta_{Y,k}\gamma_{X,k})] \\ &\quad - \frac{z^{M_{X,k}}F_{X,k,2}(z)\sum_{j=1}^{M_{X,k}}\pi^{j}_{X,k,0}\Omega_{X,k}(z)^{M_{X,k}-j}}{z^{M_{X,k}} - F_{X,k,2}(z)(z\Omega_{X,k}(z))^{M_{X,k}}}\end{aligned} \tag{28}$$

The sum of the GFs for the frame queue length after all frame transmissions within the service period can be expressed as follows:

$$\begin{aligned}\Pi_{X,k,tot}(z) &= \sum_{\mu=1}^{M_{X,k}}\Pi_{X,k,\mu}(z) \\ \Pi_{X,k,tot}(z) &= \frac{\Omega_{X,k}(z)}{1-\Omega_{X,k}(z)^{M_{X,k}}} \\ &\quad \cdot \left[Q^{+}_{X,k}(z)(1-\Omega_{X,k}(z)) - \sum_{j=1}^{M_{X,k}-1}\pi^{j}_{X,k,0}\right. \\ &\quad \left. + \sum_{j=1}^{M_{X,k}-1}\pi^{j}_{X,k,0}\Omega_{X,k}(z)^{M_{X,k}-j}\right]\end{aligned} \tag{29}$$

Now, let's formulate the probability that the node buffer is empty after the TXOP service. For the function $Q^{+}_{X,k}(z)$ to be analytic within the range $|z| < 1$, it is crucial for the zeros of the polynomials in both the denominator and the numerator to be identical. According to Rouché's theorem, the count of roots of the denominator is $M_{X,k}$. Clearly, $z = 1$ is one of the roots; the remaining $M_{X,k} - 1$ roots can be determined using Lagrange's theorem [28], as follows:

$$\begin{aligned}z_{X,k,j} &= \sum_{X=1}^{\infty}\frac{e^{2\pi j(n+1)\sqrt{-1}/M_{X,k}}}{(n+1)!} \\ &\quad \cdot \frac{d^{n-1}}{dz^{n-1}}(F_{X,k,2}(z)(A_{X,k}(z)errfr(z))^{M_{X,k}})^{\frac{n+1}{M_{X,k}}}\end{aligned} \tag{30}$$

where $j = 1 \,..\, M_{X,k} - 1$ is the index of the root. Upon substituting these $M_{X,k} - 1$ roots in the numerator of (28), we derive a set of equations for each traffic class k as

$$\begin{aligned}0 &= z_{X,k,j}F_{X,k,3}(z_{X,k,j})\upsilon^{0}_{X,k,0} \\ &\quad \cdot \sum_{\mu=1}^{M_{X,k}}\pi^{\mu}_{X,k,0}[\sigma_{Y,k}f^{aifs_{X,k}}_{X,0} + (1-\sigma_{Y,k}f^{aifs_{X,k}}_{X,0})]F_{X,k,2}(z_{X,k,j})\end{aligned}$$

$$+ (F_{X,k,0}(z_{X,k,j}) - \upsilon^0_{X,k,0}) \cdot \sum_{\mu=1}^{M_{X,k}} \pi^{\mu}_{X,k,0}[\delta_{Y,k}\gamma_{X,k} + (1-\delta_{Y,k}\gamma_{X,k})F_{X,k,1}(z_{X,k,j})] - F_{X,k,2}(z_{X,k,j}) \sum_{j=1}^{M_{X,k}} \pi^{j}_{X,k,0}\Omega_{X,k}(z_{X,k,j})^{(M_{X,k}-j)} \tag{31}$$

The final set of equations, the $M_{X,k}$-th, is obtained by imposing the condition that the cumulative mass probabilities of the buffer queue length across all observation points sum up to 1, expressed as $Q^+_{X,k}(1) + \Pi^+_{X,k,tot}(1) = 1$. Yet, to ascertain $Q^+_{X,k}(1)$ and $\Pi^+_{X,k,tot}(1)$, the application of l'Hôpital's rule leads to

$$\begin{aligned} &M_{X,k}(1-\rho'_{X,k}) - \lambda_{X,k}F'_{X,k,2}(1) \\ &= \sum_{\mu=1}^{M_{X,k}} \pi^{\mu}_{X,k,0}(M_{X,k}+1) \\ &\cdot \big[\upsilon^0_{X,k,0} + \lambda_{X,k}\upsilon^0_{X,k,0}F'_{X,k,3}(1) \\ &\quad + \lambda_{X,k}\upsilon^0_{X,k,0}F'_{X,k,2}(1)(1 - f^{aifs_{X,k}}_{X,0}\sigma_{Y,k}) \\ &\quad + \lambda_{X,k}F'_{X,k,0}(1) - \lambda_{X,k}F'_{X,k,2}(1) \\ &\quad + (1-\upsilon^0_{X,k,0})\lambda_{X,k}F'_{X,k,1}(1)(1-\delta_{Y,k}\gamma_{X,k})\big] \\ &\quad + (\lambda_{X,k}F'_{X,k,2}(1) + (1-\rho') \sum_{\mu=1}^{M_{X,k}-1} \pi^{\mu}_{X,k,0}(M_{X,k}-\mu)) \end{aligned} \tag{32}$$

where $\rho'_{X,k}$ signifies the scaled offered load, incorporating transmission failures. In no fallback case, $\rho'_{X,k}$ for legacy and NGV devices can be defined as

$$\rho'_{X,k} = \lambda_{X,k}(ld_{Y,k} + ack + 3sifs) + (1-\sigma_{Y,k}) \tag{33}$$

Similarly, we can derive $\rho'_{X,k}$ for both types of devices in the fallback case as follows

$$\begin{aligned} \rho'_{L,k} &= \lambda_{L,k}(ld_{s,k} + ack + 3sifs) + (1-\sigma_{s,k}) \\ \rho'_{N,k} &= \lambda_{N,k}(ld_{b,k} + ld_{p,k} + ack + 4sifs) + (1-\sigma_{Y,k}) \end{aligned} \tag{34}$$

The PGF for the number of frames transmitted, encompassing both successful transmissions and failures, throughout the TXOP service period, can be computed as

$$\Phi_{N,k}(z) = \frac{1}{\Pi_{N,k,tot}(1)} \cdot \left[\sum_{\mu=1}^{M_{N,k}-1} \pi^{\mu}_{N,k,0}z^{\mu} + z^{M_{N,k}} \left(\Pi_{N,k,tot}(1) - \sum_{\mu=1}^{M_{N,k}-1} \pi^{\mu}_{N,k,0}\right)\right] \tag{35}$$

VII. MARKOV CHAIN MODEL

The complete Markov chain for a single traffic class is depicted in Figure 3. A Markov chain illustrates the behavior of the CSMA/CA algorithm in the context of both legacy and NGV devices, encompassing four distinct traffic classes. It represents a stochastic process characterized by a stationary distribution of states, denoted as $y_{X,k,i,j,b}$. Here, the symbol $X \in (L, N)$ denotes legacy and NGV devices, respectively. Additionally, the variable $k = 0\,..\,3$ denotes the traffic category, while $i = 0\,..\,m_{X,k}$ denotes the specific backoff phase index. The variable $j = 0\,..\,W_{X,k,i} - 1$ represents the value of the backoff counter, while $b = 0\,..\,B_{X,k}$ is the freezing counter value. In this specific Markov chain, state transitions can occur only during an idle state in the medium and when a particular requirement is met. Even though the zeroth backoff process must be performed irrespective of the buffer's occupancy, we have presented distinct zeroth backoff sequences for when the buffer is empty (depicted as a vertical sequence of backoff states) and when it is not (displayed as the first horizontal row of backoff states). This duplication aims to clarify the transition into the idle state. The probability of entering the vertical zeroth backoff stage is denoted as

$$Pp_{X,k} = \tau_{Y,k}\gamma_{X,k}\delta_{Y,k}\pi^*_{X,k,0} \tag{36}$$

Here, $\tau_{Y,k}$ represents the transmission probability in the primary, secondary, and wide channels. Within our model, $\pi^*_{X,k,0}$ represents the connection between the queuing and Markov chain models that can be defined as follows

$$\pi^*_{X,k,0} = \frac{\sum_{\mu=1}^{M_{X,k}} \pi^{\mu}_{X,k,0}}{\Pi_{X,k,tot}(1)} \tag{37}$$

The standard requires that nodes initiate a proactive backoff of $W_{X,k,0}$ immediately following a successful transmission, even in the absence of data in the node's buffer. To depict this situation, we have employed states denoted as $y_{X,k,i,j,b}$, where $i = -2$ and j ranges from 0 to $W_{X,k,0} - 1$. When the node buffer remains empty after the backoff count, the node transitions into the idle state. The probability of entering the idle state is denoted as $\tau_{Y,k}\delta_{Y,k}\gamma_{X,k}\pi^*_{X,k,0}\upsilon^0_{X,k,0}$.

To calculate the count of frame arrivals during the frame service time, we suppose that these arrivals follow a Poisson process with a frame arrival rate denoted as $\lambda_{X,k}$. This means that the inter-arrival time between consecutive frame arrivals follows an exponential distribution with the parameter $\lambda_{X,k}$. The PGF for the number of arrivals within a fixed time interval, which in this case corresponds to the frame service time, is achieved from this exponential distribution. Referring to the branching behavior observed in the Markov chain illustrated in Figure 3, we can express the LST for the distance between two service periods in terms of backoff slots as

$$D^*_{X,k}(s) = St_{X,k}(e^{-s})\{\pi^*_{X,k,0}B_{X,k,0}(e^{-s})\upsilon^0_{X,k,0}\frac{\lambda_{X,k}}{\lambda_{X,k}+s}$$

$$\cdot \left[f_{X,0}^{AIFS_{X,k}}\sigma_{Y,k} + (1 - f_{X,0}^{AIFS_{X,k}}\sigma_{Y,k})Bof_{X,k}(e^{-s})\right] + \pi^*_{X,k,0}(1 - \upsilon^0_{X,k,0})B_{X,k,0}(e^{-s})\delta_{Y,k}\gamma_{X,k} + (1-\delta_{Y,k}\gamma_{X,k}Bzof_{X,k}(e^{-s}))(1-\pi^*_{X,k,0})Bof_{X,k}(e^{-s})\Big\} \quad (38)$$

When there is no data in the node buffer, the frame service time is determined by subtracting the waiting time for the arrival of the frame.

$$Tt^*_{X,k}(s) = St_{X,k}(e^{-s})\Big\{\pi^*_{X,k,0}B_{X,k,0}(e^{-s})\upsilon^0_{X,k,0} \cdot \left[f_{X,0}^{AIFS_{X,k}}\sigma_{Y,k} + (1 - f_{X,0}^{AIFS_{X,k}}\sigma_{Y,k})Bof_{X,k}(e^{-s})\right] + \pi^*_{X,k,0}(1 - \upsilon^0_{X,k,0})B_{X,k,0}(e^{-s})\delta_{Y,k}\gamma_{X,k} + (1-\delta_{Y,k}\gamma_{X,k}Bzof_{X,k}(e^{-s}))(1-\pi^*_{X,k,0})Bof_{X,k}(e^{-s})\Big\} \quad (39)$$

In this context, $\upsilon^0_{X,k,0}$ is defined as $B^*_{X,k,0}(\lambda_{x,k})$, where $B^*_{X,k,0}(s) = B_{X,k,0}(e^{-s})$ signifies the probability of no frame arrivals during the zeroth backoff on the corresponding channels. The mean value of $Tt^*_{X,k}(s)$ is $\overline{Tt_{X,k}} = \frac{dTt^*_{X,k}(s)}{ds}$.

Probability that a device remains idle as

$$P_{X,k,idle} = 1 - \frac{\overline{Tt_{X,k}}}{\overline{D_{X,k}}} \quad (40)$$

The probability of entering the idle state occurs when the node's buffer remains empty after the proactive backoff countdown. This state persists until a new frame arrives. If the medium is found to be idle upon leaving the idle state, a freezing countdown is initiated. When the countdown reaches zero and the medium is still idle, the frame transmission commences. However, if the medium becomes busy during the freezing countdown, a new backoff phase is triggered.

The probability of detecting an idle medium is denoted as $f_{X,0}$, while the probability of encountering no collision is labeled as $\gamma_{X,0}$ for each access category and for legacy and NGV devices. In the final state of the block, access is achieved with a probability of $y_{X,k,0} = Pp_{X,k}\upsilon^0_{X,k,0}f_{X,0}^{AIFS_{X,k}}$. The sum of probabilities within the initial freezing block following the idle state, initiated during active medium conditions, is expressed as:

$$S_{X,k,-1} = Pp_{X,k}\upsilon^0_{X,k,0}\sum_{i=0}^{AIFS_{X,k}} f^i_{X,0} \quad (41)$$

After the initial proactive backoff phase, known as the "zeroth" phase, the access to the medium occurs with a probability represented by $y_{X,k,-2,0,0} = Pp_{X,k}$ (1 - $\upsilon^0_{X,k,0}$). The sum of probabilities within the proactive zeroth backoff phase, which initiates with an empty buffer when i = −2, is calculated as follows:

$$S_{X,k,-2} = \frac{Pp_{X,k}}{W_{X,k,0}}[Fl_{X,k} + (Fl_{X,k}+1)(W_{X,k,0}-1) + 0.5(1 + (1-\gamma_{X,k})Fl_{X,k})(W_{X,k,0}-1) .(W_{X,k,0}-2)] \quad (42)$$

The input probability for each block of the zeroth backoff phase, which is initiated when the buffer is not empty, can be acquired as

$$Pin_{X,k,0} = \frac{1}{W_{X,k,0}}[\tau_{Y,k}\gamma_{X,k}\delta_{Y,k}(1-\pi^*_{X,k,0}) + y_{X,k,m_{X,k},0,0}(1-\gamma_{X,k}\delta_{Y,k}) + Pp_{X,k}\upsilon^0_{X,k,0}(1 - f_{X,k}^{AIFS_{X,k}}\sigma_{Y,k}) + Pp_{X,k}(1-\upsilon^0_{X,k,0})\gamma_{X,k}\delta_{Y,k}(1-\pi^*_{X,k,0})] \quad (43)$$

where $y_{X,k,m_k,0,0}$ can be computed as

$$y_{X,k,m_{X,k},0,0} = \frac{\tau_{Y,k}\gamma_{X,k}\delta_{Y,k}(1-\gamma_{X,k}\delta_{Y,k})^R}{1-(1-\gamma_{X,k}\delta_{Y,k})^{R+1}} \quad (44)$$

The state within the initial backoff phase can occur under the following circumstances: when the buffer remains occupied after the zeroth proactive backoff, when a transmission attempt after the zeroth proactive phase fails, or when the freezing counter fails to complete successfully after exiting the idle state. The corresponding input probability is thus calculated as:

$$Pin_{X,k,1} = \frac{1}{W_{X,k,1}}[Pin_{X,k,0}W_{X,k,0}(1-\gamma_{X,k,0}\delta_{Y,k}) + Pp_{X,k}(1-\upsilon^0_{X,k,0})(1-\gamma_{X,k}\delta_{Y,k})] \quad (45)$$

The input probability for each block during the i-th backoff attempt, where i ranges from 2 to R, can be derived as:

$$Pin_{X,k,l} = Pin_{X,k,1}W_{X,k,1}\frac{(1-\gamma_{X,k}\delta_{Y,k})^{l-1}}{W_{X,k,l}} \quad (46)$$

The access probability after each horizontal backoff stage is denoted as $y_{X,k,i,0,0} = Pin_{X,k,i}$ when $i = 0\,..\,R$. The normalization condition can be expressed as follows:

$$1 = S_{X,k,-2} + P_{X,k,idle} + S_{X,k,-1} + Fl_{X,k}\sum_{i=0}^{R} Pin_{X,k,i} + 0.5(1 + (1-g_{X,k})Fl_{X,k}) \cdot \sum_{i=0}^{R}(W_{X,k,i}-2)(W_{X,k,i}-1)Pin_{X,k,i} + (Fl_{X,k}+1)\sum_{i=0}^{R}(W_{X,k,i}-1)Pin_{X,k,i} \quad (47)$$

Due to the interconnected nature of all nodes through their participation in the medium, it was essential to tackle a system comprising eight equation subsystems. Each subsystem corresponds to the Markov chain associated with a particular pairing of device types labeled as X and traffic class represented as k. This strategy enabled us to calculate the values for $\gamma_{X,k}$, $f_{X,k}$, and $\tau_{Y,k}$.

If we consider the frames that arrived during the frame service time, the total response time can be computed, as the

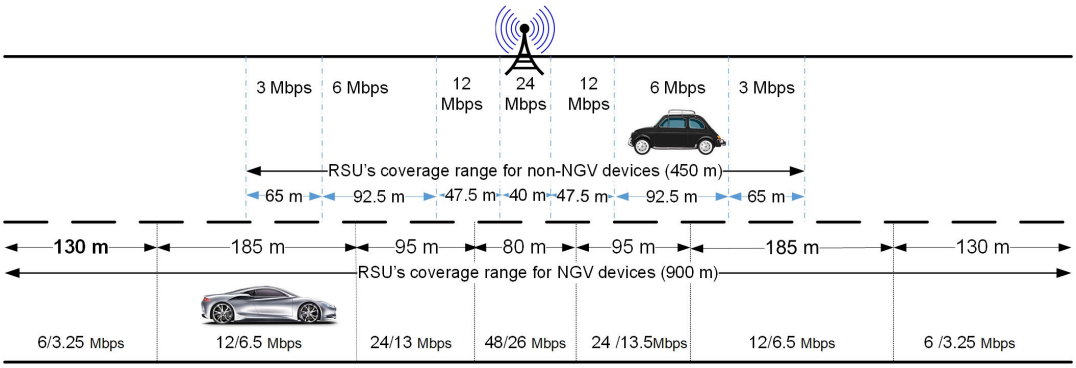

FIGURE 4. Data rates are affected by distance, particularly in a road segment with a central Roadside Unit (RSU).

number of frames remaining after the departure of a frame is equivalent to the number of frames that arrived while the target frame was in the system. If we denote the LST of the response time for each traffic class in their corresponding channels as $W^*_{X,k}(s)$, the PGF for the number of frames left after a frame departure can be expressed as

$$\frac{\Pi_{X,k,tot}(z)}{\Pi_{X,k,tot}(1)} = W^*_{X,k}(\lambda_{x,k} - z\lambda_{x,k})z\Omega_{X,k}(z) \tag{48}$$

Because of the PASTA (Poisson Arrivals See Time Averages) property of M/G/1 systems, the distribution probability of the number of frames in the system at the time of arrival is identical to the distribution of the number of frames in the system at any arbitrary time. Hence, $\Pi_{X,k}(z)$ also shows the distribution probability of buffer occupancy at an arbitrary time, allowing for the analysis of buffer occupancy probabilities at different time instances within the M/G/1 system. By substituting $s = \lambda_{x,k} - \lambda_{x,k}z$, we derive the LST of the waiting time as:

$$W^*_{X,k}(s) = \frac{\Pi_{X,k,tot}(1 - \frac{s}{\lambda_{x,k}})}{(1 - \frac{s}{\lambda_{x,k}})\Pi_{X,k,tot}(1)\Omega_{X,k}(1 - \frac{s}{\lambda_{x,k}})} \tag{49}$$

and its mean value is

$$\overline{W_{X,k}} = \frac{1}{\lambda_{X,k}}[\frac{\Pi'_{X,k,tot}(1)}{\Pi_{X,k,tot}(1)} - \rho'_{X,k}] \tag{50}$$

VIII. PERFORMANCE EVALUATION

We assessed the influence of TXOP allocation on low-priority access categories of legacy devices and examined the impact of distance on IEEE 802.11bd channel bonding, considering scenarios with and without fallback for both non-NGV and NGV devices. This evaluation was conducted using an analytical model solved through Maple from Maplesoft, Inc. Our study involved the modeling of NGV and legacy STAs, categorizing them into four traffic classes denoted as $AC_{X,k}$ where k = 0, 1, 2, 3 respectively, based on distinct priorities.

For both legacy and NGV devices, frames of access class k followed a Poisson process with uniform arrival rates $\lambda_{X,k} = \lambda$, measured in packets per second per station. However, the bit error rate varied depending on the channel type: $ber_{L,k} = 2 \cdot 10^{-6}$ for legacy devices and $ber_{N,k} = 5 \cdot 10^{-6}$ for NGV STAs.

Maintaining a consistent packet size of 500 bytes for both non-NGV and NGV devices, the duration of packets varied due to differences in data rates and, potentially, the distance between the vehicle and the RSU. We assumed each access class, for both legacy and NGV standards, consisted of five devices. In addition, our analysis encompassed the operation of NGV devices across all access categories and legacy devices specifically for low-priority traffic classes, both with and without fallback, with the maximum number of frames when TXOP is employed set at $M_{X,k} = 2$ or 4.

In our experimentation, we consider distance as depicted in Figure4. Lower data rates lead to prolonged packet transmission times. To ensure a varied set of results, we have strategically distributed devices uniformly at different distances from the RSU. Key parameter values for both legacy and NGV devices are summarized in Table 1.

In all Figures, the top row diagrams showcase outcomes when NGV devices refrain from utilizing fallback, whereas the bottom row diagrams illustrate corresponding results with fallback. **In each diagram, results for legacy devices are illustrated using symbols: black crosses for AC0, blue squares for AC1, red circles for AC2, and green diamonds for AC3. Conversely, outcomes for NGV devices are presented with lines: solid black lines for AC0, dash-dot blue lines for AC1, dashed red lines for AC2, and dotted green lines for AC3. Table 2 summarizes this notation.**

We also conducted simulations using ns3 with MX4 for both non-NGV and NGV devices. The diagrams in Figs. 6, 7, and 8 include both analytical results shown with green, red, blue, and black lines and symbols, and simulation results, shown with pink lines and symbols; as above, lines correspond to NGV devices while symbols correspond to legacy, non-NGV devices.

Figure 5 depicts the mean number of error-free frames transmitted within the TXOP service period across varying values of the TXOP limit $M_{X,k}$ for both NGV and non-NGV devices, taking into account the distance impact. Despite

TABLE 1. Parameter values.

Parameter	numerical value
backoff slot (ω)	13 μs
SIFS	32 μs
max. number of backoff attempts (R)	7
data MAC header	32 Bytes
ACK MAC header	10 Bytes
PHY header (non-NGV devices)	40 Bytes
PHY header (NGV devices)	80 Bytes
non-NGV device data rates at 10 MHz bandwidth	
distance 0 to 40 m	24 Mbps
distance 41 to 135 m	12 Mbps
distance 136 to 320 m	6 Mbps
distance 321 to 450 m	3 Mbps
NGV device data rates at 20 / 10 MHz bandwidth	
distance 0 to 80 m	48 / 26 Mbps
distance 81 to 270 m	24 / 13 Mbps
distance 271 to 640 m	12 / 6.5 Mbps
distance 641 to 900 m	6 / 3.25 Mbps

TABLE 2. Symbols in the diagrams.

device type	symbol	description
legacy	+	$AC_{L,0}$
(non-NGV)	□	$AC_{L,1}$
	○	$AC_{L,2}$
	◇	$AC_{L,3}$
NGV	———	$AC_{N,0}$
	– – – –	$AC_{N,1}$
	– · – · – ·	$AC_{N,2}$
	. . . . .	$AC_{N,3}$

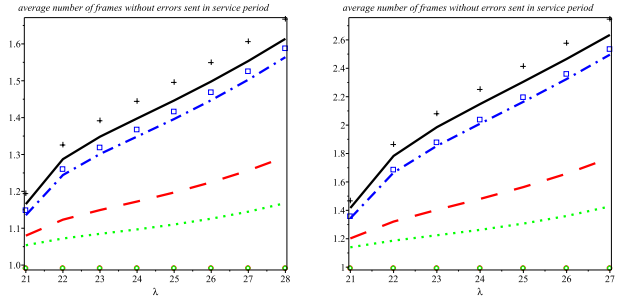

(a) TXOP limit $M = 2$, NGV devices don't use fallback.

(b) TXOP limit $M = 4$, NGV devices don't use fallback.

(c) TXOP limit $M = 2$, NGV devices use fallback.

(d) TXOP limit $M = 4$, NGV devices use fallback.

FIGURE 5. Mean number of frames sent per TXOP period.

the uniform TXOP allocation for all traffic classes of NGV devices and the two lower-priority classes of legacy devices, minimal enhancements are observed for $AC_{X,0}$ and $AC_{X,1}$

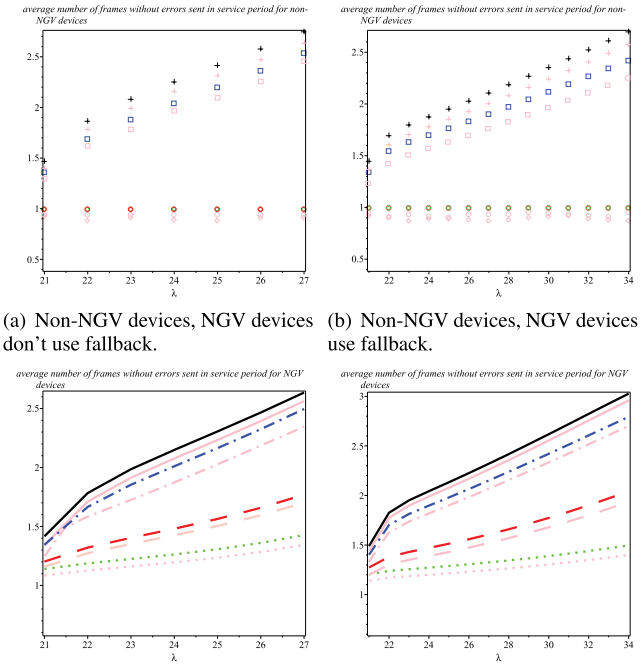

(a) Non-NGV devices, NGV devices don't use fallback.

(b) Non-NGV devices, NGV devices use fallback.

(c) NGV devices (without fallback).

(d) NGV devices (with fallback).

FIGURE 6. Mean number of frames sent per TXOP period when $M = 4$. Top row: results for legacy devices; bottom row: results for NGV devices. Pink symbols and lines denote simulation results.

with increased allocation. Conversely, NGV higher-priority classes exhibit only slight to moderate improvements in throughput.

While low-priority traffic classes of NGV devices outperform their counterparts from legacy devices in scenarios without fallback, it is noteworthy that low-priority traffic classes of non-NGV devices exhibit superior performance compared to their NGV counterparts when fallback mechanism is in place. This may be attributed to the suspension of the target station's arbitration counters and backoff counter throughout the TXOP periods, applying to all nodes attempting to access the medium during the target station's backoff process. The protracted duration of the arbitration countdown enhances the likelihood of NGV higher-priority traffic classes obtaining access during the target station's arbitration countdown. The prolonged countdown period creates additional opportunities for other traffic classes to access the medium while the target station is in the arbitration and countdown phase.

Mean waiting time in the device queue is depicted in Figure 7. As can be seen, there is discernible prioritization of traffic classes, with packets from higher-priority classes experiencing significantly shorter waiting times compared to those from lower-priority classes for both types of devices, regardless of whether NGV devices utilize fallback or not.

In both scenarios, the mean waiting time tends to decrease as the value of $M_{X,k}$ in the network increases for both types of devices. When there is no fallback, mean waiting times for NGV devices are marginally lower than the corresponding values for legacy devices.

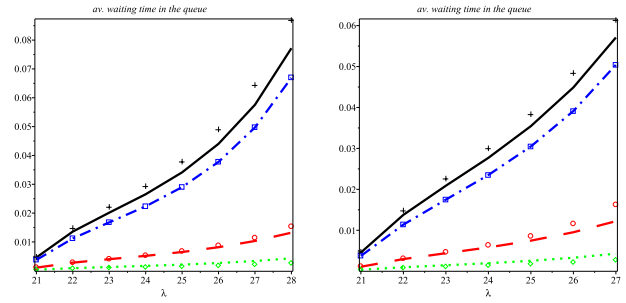

(a) TXOP limit $M = 2$, NGV devices don't use fallback. (b) TXOP limit $M = 4$, NGV devices don't use fallback.

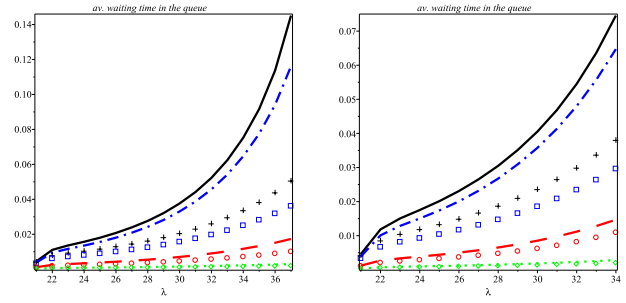

(c) TXOP limit $M = 2$, NGV devices use fallback. (d) TXOP limit $M = 4$, NGV devices use fallback.

FIGURE 7. Mean waiting time in the device queue.

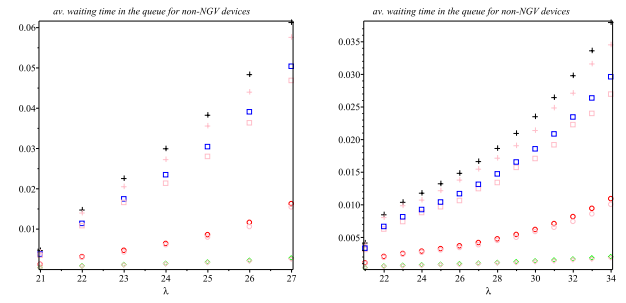

(a) Non-NGV devices, NGV devices don't use fallback. (b) Non-NGV devices, NGV devices use fallback.

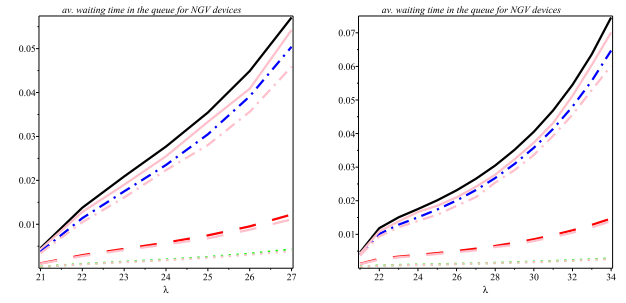

(c) NGV devices (without fallback). (d) NGV devices (with fallback).

FIGURE 8. Mean waiting time when TXOP limit is $M = 4$. Pink symbols and lines denote simulation results.

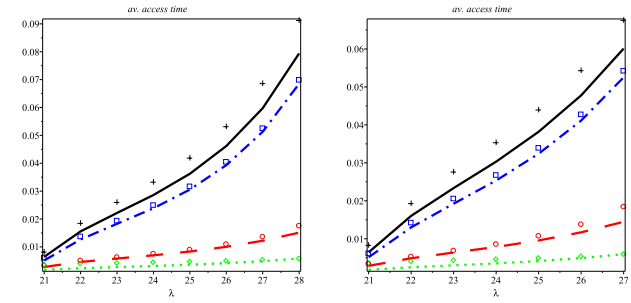

(a) TXOP limit $M = 2$, NGV devices don't use fallback. (b) TXOP limit $M = 4$, NGV devices don't use fallback.

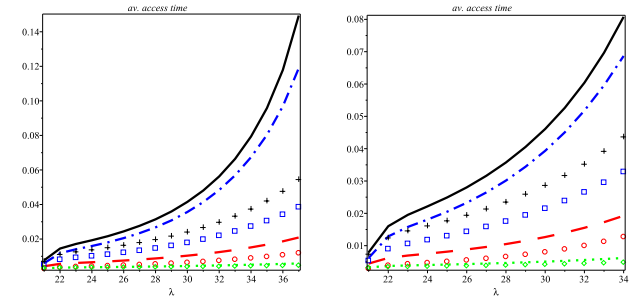

(c) TXOP limit $M = 2$, NGV devices use fallback. (d) TXOP limit $M = 4$, NGV devices use fallback.

FIGURE 9. Mean access time.

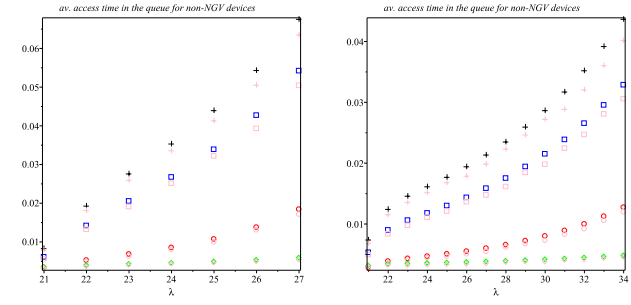

(a) Non-NGV devices, NGV devices don't use fallback. (b) Non-NGV devices, NGV devices use fallback.

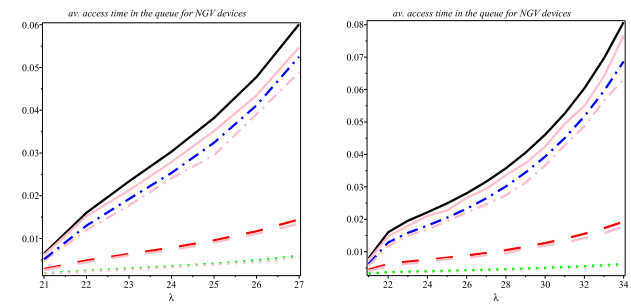

(c) NGV devices (without fallback). (d) NGV devices (with fallback).

FIGURE 10. Mean access time when TXOP limit is $M = 4$. Pink symbols and lines denote simulation results.

In the case where NGV devices employ fallback mechanisms, legacy lower-priority traffic experiences shorter waiting times, especially at higher TXOP limits. However, mean waiting times for higher-priority classes AC_2 and AC_3 for legacy and NGV devices are approximately equal when comparing legacy and NGV devices with fallback.

Figure 9 illustrates the mean access time for different access categories in both scenarios. The results indicate that

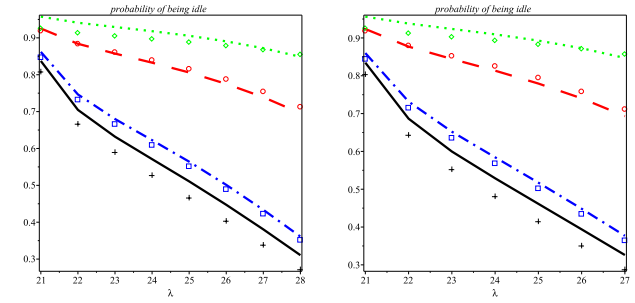

(a) TXOP limit $M = 2$, NGV devices don't use fallback.

(b) TXOP limit $M = 4$, NGV devices don't use fallback.

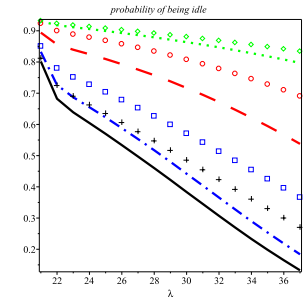

(c) TXOP limit $M = 2$, NGV devices use fallback.

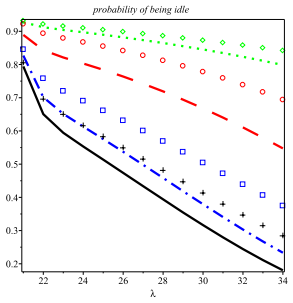

(d) TXOP limit $M = 4$, NGV devices use fallback.

FIGURE 11. Idle probability.

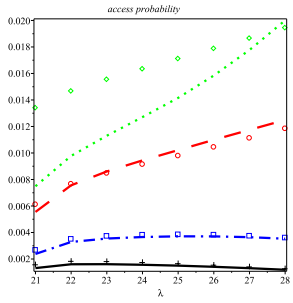

(a) TXOP limit $M = 2$, NGV devices don't use fallback.

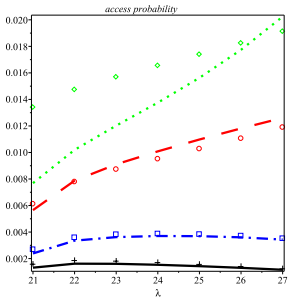

(b) TXOP limit $M = 4$, NGV devices don't use fallback.

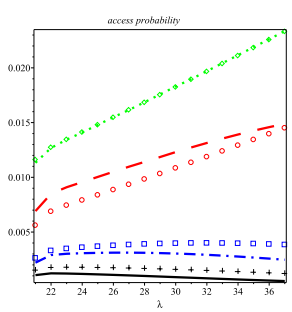

(c) TXOP limit $M = 2$, NGV devices use fallback.

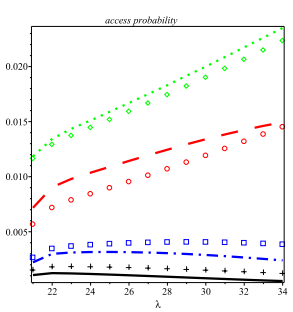

(d) TXOP limit $M = 4$, NGV devices use fallback.

FIGURE 12. Access probability.

traffic classes originating from NGV devices outperform those from legacy devices in the absence of fallback mechanism, irrespective of considering the distance impact and the increase in the $M_{X,k}$ parameter. When NGV devices employ the fallback mechanism, the performance of legacy devices is further enhanced.

Notably, low-priority traffic classes (AC_0 and AC_1) demonstrate superior performance compared to NGV devices, especially at higher values of $M_{X,k}$. Conversely, the higher-priority traffic classes (AC_2 and AC_3) from legacy devices exhibit marginally improved performance as $M_{X,k}$ increases, due to the reduced medium occupancy time by NGV devices in the fallback scenario.

In both scenarios, the mean access time decreases for both legacy and NGV devices with an increase in $M_{X,k}$, considering the distance effect on the network.

Figure 11 illustrates the probability of an access category transitioning to an idle state after completing packet servicing. In scenarios with low packet arrival rates, the system predominantly remains idle. However, as the packet arrival rate increases, the probability of the medium being idle gradually diminishes. The service of up to $M_{X,k}$ packets for NGV devices and lower-priority traffic classes of legacy devices during the TXOP period contributes to a gradual decline in idle probability as the packet arrival rate rises. In this scenario, non-NGV devices do not exhibit an accelerated decrease in the idle probability in lower priority classes, and the network does not reach the saturation regime quickly in both approaches.

In instances where NGV devices employ fallback, their idle probability decreases as packet transmissions on the primary channel prolong, resulting in higher idle probability values for legacy devices compared to NGV devices. With a higher number of packets serviced per TXOP period, the low-prioritized categories of NGV devices face nearing saturation under higher traffic loads. NGV devices operating on the wide channel without fallback achieve higher efficiency as their idle probability remains elevated. Across all cases, it is evident that EDCA traffic prioritization leads to higher idle probability values for traffic classes with higher priority, both for legacy and NGV devices.

Figure 12 illustrates the medium access probability. As the packet arrival rate increases, devices attempt to access the medium more frequently, leading to a gradual rise in access probability. In the scenario without fallback, legacy devices outperform NGV devices because NGV devices require both the primary and secondary channels to be idle before accessing the medium, while non-NGV devices only utilize the secondary channel. However, the performance of NGV STAs in higher-priority traffic classes improves with increasing packet arrival rate and TXOP limit, taking into account the distance effect on the network.

Conversely, when NGV devices operate with fallback, their access probability improves, especially in higher-priority traffic classes, as switching to operation on the primary channel effectively separates their transmission from that of a legacy device on the secondary channel. As before, access probability for NGV devices improves with an increase in the TXOP limit, and we consider the distance effect on them.

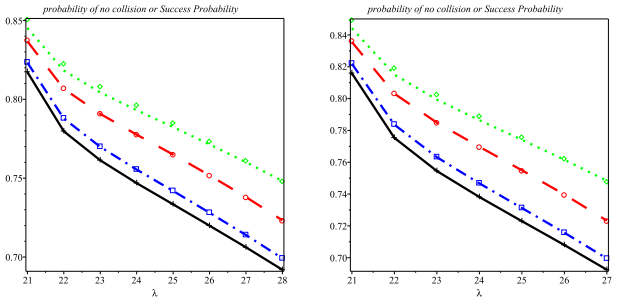

(a) TXOP limit $M = 2$, NGV devices don't use fallback.

(b) TXOP limit $M = 2$, NGV devices don't use fallback.

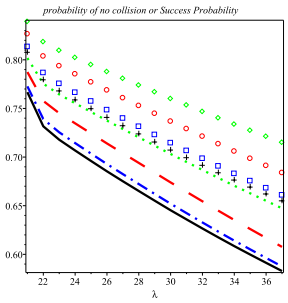

(c) TXOP limit $M = 2$, NGV devices use fallback.

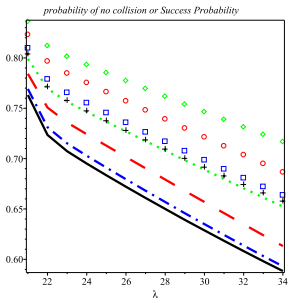

(d) TXOP limit $M = 4$, NGV devices use fallback.

FIGURE 13. Success probability.

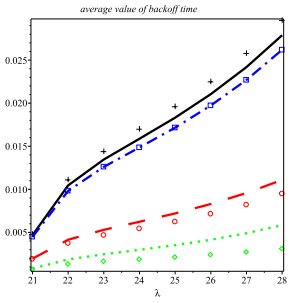

(a) TXOP limit $M = 2$, NGV devices don't use fallback.

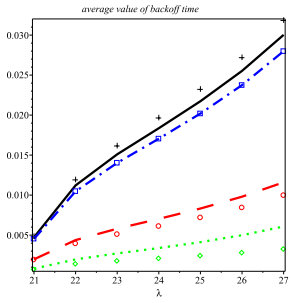

(b) TXOP limit $M = 4$, NGV devices don't use fallback.

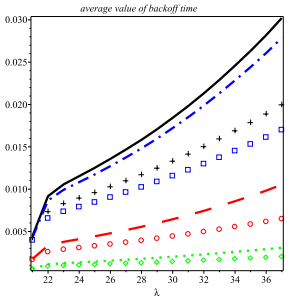

(c) TXOP limit $M = 2$, NGV devices use fallback.

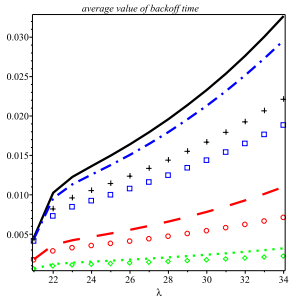

(d) TXOP limit $M = 4$, NGV devices use fallback.

FIGURE 14. Mean backoff time.

Figure 13 depicts the probability of successfully transmitting a frame. In instances where NGV devices refrain from using fallback, the performance disparity between legacy and NGV devices is minimal, particularly under low traffic loads, especially at higher TXOP limit values. Interestingly, the success probability for NGV devices utilizing fallback is slightly inferior to that of non-NGV devices.

The diagrams presented in Figure 14 show mean backoff time. As can be seen, higher-priority traffic classes of non-NGV and NGV devices, namely AC_3 and AC_2, employ smaller AIFS and contention window settings, and their mean backoff times tend to be significantly shorter than those observed for lower-priority classes. The difference is less noticeable at lower packet arrival rates because backoff procedures end sooner due to reduced contention, but it become more pronounced as packet arrival rate increases, for both legacy and NGV devices. Legacy devices generally outperform NGV devices that don't use fallback, esp. for higher-priority traffic classes, and also NGV devices that use fallback.

Figure 15 illustrates the probability of the device buffer being empty after packet departure for various $M_{X,k}$ values, distinguishing between NGV and non-NGV STAs. NGV devices, without fallback, outperform their legacy counterparts across all traffic classes, particularly when the TXOP limit is higher. However, with fallback in use, legacy devices demonstrate superior performance in all traffic categories, especially in lower-priority traffic.

For both NGV and non-NGV devices, high-priority access categories are more likely to have an empty buffer after packet departure due to shorter backoff times. In contrast, lower-priority access classes experience longer backoff times, resulting in a different performance scenario.

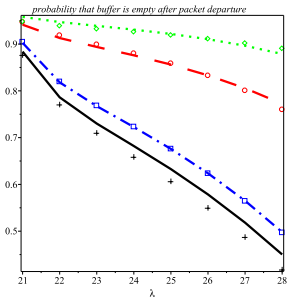

(a) TXOP limit $M = 2$, NGV devices don't use fallback.

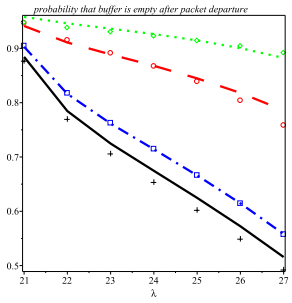

(b) TXOP limit $M = 4$, NGV devices use fallback.

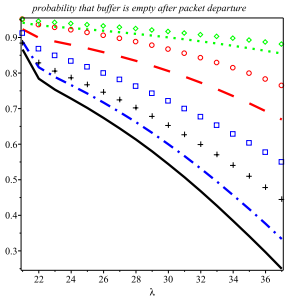

(c) TXOP limit $M = 2$, NGV devices use fallback.

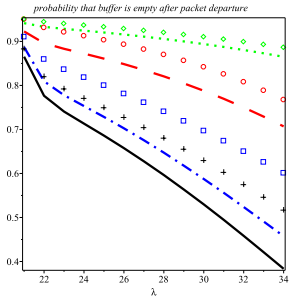

(d) TXOP limit $M = 4$, NGV devices use fallback.

FIGURE 15. Empty buffer probability.

We note that the simulation results are very close to those obtained from the analytical model, which confirms the validity of the analytical model as an accurate representation of the behavior of IEEE 802.11bd networks with coexisting NGV and legacy devices.

IX. CONCLUSION

Our study investigates the performance of both NGV and legacy, non-NGV devices in V2X communication that bridge the transition from IEEE 802.11p to IEEE 802.11bd standards. By introducing an analytical framework combining queuing analysis and Markov chain analysis, we have addressed the complexities of TXOP allocation in coexisting legacy and NGV device environments. Our findings underscore the importance of balanced TXOP allocation for efficient communication, with observed improvements in throughput for NGV devices and consideration of vehicle-to-RSU distance. Moreover, our analysis of EDCA saturation states and the impact of RSU transmission coverage highlights the necessity of aligning network parameters to prevent saturation and ensure seamless integration of diverse device types.

Our future research will delve into exploring the practical applications of IEEE 802.11bd communication technology across different scenarios and optimizing parameter values based on specific road conditions and application needs.

APPENDIX. MODELING THE BACKOFF PROCESS

PGF for the successful transmission duration on the secondary and wide channels by legacy and NGV devices without fallback, respectively, during the period $A_{X,r}$, where $r = 0$ to 3, can be formulated as

$$Sw_{X_{w0},r} = \frac{\sum_{i=r}^{3} n_{L,i}\tau_{s,i}St_{L_{w0},i} + \sum_{j=r}^{3} n_{N,j}\tau_{b,j}St_{N_{w0},j}}{\sum_{i=r}^{3} n_{L,i}\tau_{s,i} + \sum_{j=r}^{3} n_{N,j}\tau_{b,j}} \tag{51}$$

While the PGFs correspond to the scenario where NGV devices utilize fallback in both legacy and NGV devices can be expressed as

$$Sw_{L_w,r} = \frac{\sum_{i=r}^{3} n_{L,i}\tau_{s,i}St_{L_w,i} + \sum_{j=r}^{3} n_{j}\tau_{b,j}St_{N_w,j}}{\sum_{i=r}^{3} n_{L,i}\tau_{s,i} + \sum_{j=r}^{3} n_{N,j}\tau_{b,j}} \tag{52}$$

$$Sw_{N_w,r} = \frac{\sum_{i=r}^{3} n_{L,i}\tau_{s,i}St_{L_w,i}}{\sum_{i=r}^{3} n_{L,i}\tau_{s,i} + \sum_{j=r}^{3}(P_{b,j}n_{N,j}\tau_{b,j} + Q_{p,j}n_{N,j}\tau_{p,j})} + \frac{\sum_{j=r}^{3}(P_{b,j}n_{N,j}\tau_{b,j} + Q_{p,j}n_{N,j}\tau_{p,j})St_{N_w,j}}{\sum_{i=r}^{3} n_{L,i}\tau_{s,i} + \sum_{j=r}^{3}(P_{b,j}n_{N,j}\tau_{b,j} + Q_{p,j}n_{N,j}\tau_{p,j})} \tag{53}$$

When NGV devices don't use fallback, the probabilities $Pa_{x,l}$ that freezing counters of non-NGV and NGV STAs with $AC_{x,k} < l$ will be restarted due to successful transmission on secondary and wide channels in the period $A_{x,l}$, where $l = 1 \ldots 3$, are

$$Pa_{X_{wo},l} = \left(\sum_{i=l}^{3} \frac{n_{L,i}\tau_{s,i}}{1-\tau_{s,l}} + \sum_{j=l}^{3} \frac{n_{N,j}\tau_{b,j}}{1-\tau_{b,j}}\right) \cdot \prod_{i=l}^{3}(1-\tau_{s,l})^{n_{L,l}} \prod_{j=l}^{3}(1-\tau_{b,j})^{n_{N,j}} \tag{54}$$

so that probability of their arbitration counters restarting due to collision is $Pc_{X_{wo},l} = 1 - f_{X,l} - Pa_{X_{wo},l}$, $l = 1 \ldots 3$.

Likewise, the probability that arbitration counters of both legacy and NGV devices employing fallback will restart due to successful transmissions on secondary, wide, and primary channels during the period $A_{x,l}$, where $l = 1 \ldots 3$, can be derived as

$$Pa_{L_w,l} = \left(\sum_{i=l}^{3} \frac{n_{L,i}\tau_{s,i}}{1-\tau_{s,l}} + \sum_{j=l}^{3} \frac{n_{N,j}\tau_{b,j}}{1-\tau_{b,j}}\right) \cdot \prod_{i=l}^{3}(1-\tau_{s,l})^{n_{L,l}} \prod_{j=l}^{3}(1-\tau_{b,j})^{n_{N,j}}$$

$$Pa_{N_w,l} = \left(\sum_{i=l}^{3} \frac{n_{L,i}\tau_{s,i}}{1-\tau_{s,l}} + \sum_{j=l}^{3} \frac{n_{N,j}(P_{b,j}\tau_{b,j} + Q_{p,j}\tau_{p,j})}{P_{b,j}(1-\tau_{b,j})Q_{p,j}(1-\tau_{p,j})}\right) \cdot \prod_{i=l}^{3}(1-\tau_{s,l})^{n_{L,l}} \prod_{j=l}^{3} P_{b,j}(1-\tau_{b,j})^{n_{N,j}} Q_{p,j}(1-\tau_{p,j})^{n_{N,j}} \tag{55}$$

while probability of the arbitration counters in legacy and NGV devices restarting due to collision can be expressed as $Pc_{X_w,l} = 1 - f_{X,l} - Pa_{X_w,l}$, $l = 1 \ldots 3$.

When $k = 3$, the arbitration counter does not undergo a restart. Therefore, $AC_{X,3}$ must traverse through $AIFSN_{X,3}$ slots before initiating transmission. As the result, PGF for the time duration spent in the arbitration countdown can be expressed as

$$Bfnl_{X,3} = z^{AIFSN_{X,3}} \tag{56}$$

The generalized form for the PGF of the freezing countdown time is

$$Bfnl_{X,k} = \frac{Bfnln_{X,k}}{Bfnld_{X,k}}, k = 0 \ldots 2 \tag{57}$$

where $Bfnln_{X,k} = z^{AIFSN_{X,k}} \prod_{i=k+1}^{3} (f_{X,i}z)^{A_{X,i,max}}$ and

$$Bfnld_{X,k} = 1 - \sum_{i=k+1}^{3} \frac{Pa_{X,i}Sw_{X,i}(z) + Pc_{X,i}Ct_{X,i}(z)}{1 - f_{X,i}} \cdot \sum_{n=0}^{A_{X,i,max}-1} (zf_{X,i})^n (1 - f_{X,i}) z \prod_{l=i+1}^{3} (zf_{X,i})^{A_{X,i,max}}$$

The last equations allow us to determine the PGF for the duration of the arbitration countdown.

Regular backoff countdown begins when the arbitration counter reaches zero and the medium is idle. Certainly, if any activity takes place on the medium during the backoff countdown, the countdown is interrupted and suspended. In the no-fallback approach, we can determine the probability of the backoff countdown being suspended in both legacy and NGV devices by employing the Markov chain model in the following manner:

$$Pbs_{L_{wo},k,l} = \left(\sum_{i=l}^{3} \frac{n_{L,i}\tau_{s,i}}{(1-\tau_{s,i})(1-\tau_{s,k})} + \sum_{i=l}^{3} \frac{n_{N,i}\tau_{b,i}}{(1-\tau_{b,i})(1-\tau_{s,k})} \right) \cdot \prod_{u=l}^{3} (1-\tau_{s,u})^{n_{L,u}} \prod_{u=l}^{3} (1-\tau_{b,u})^{n_{N,u}} - \frac{\tau_{s,k}}{(1-\tau_{s,k})^2} \prod_{u=l}^{3} (1-\tau_{s,u})^{n_{L,u}} \prod_{u=l}^{3} (1-\tau_{b,u})^{n_{N,u}} \tag{58}$$

$$Pbs_{N_{wo},k,l} = \left(\sum_{i=l}^{3} \frac{n_{L,i}\tau_{s,i}}{(1-\tau_{s,i})(1-\tau_{b,k})} + \sum_{i=l}^{3} \frac{n_{N,i}\tau_{b,i}}{(1-\tau_{b,i})(1-\tau_{b,k})} \right) \cdot \prod_{u=l}^{3} (1-\tau_{s,u})^{n_{L,u}} \prod_{u=l}^{3} (1-\tau_{b,u})^{n_{N,u}} - \frac{\tau_{b,k}}{(1-\tau_{b,k})^2} \prod_{u=l}^{3} (1-\tau_{s,u})^{n_{L,u}} \prod_{u=l}^{3} (1-\tau_{b,u})^{n_{N,u}} \tag{59}$$

In both cases, $l \leq k$.

The probability of the backoff counter being interrupted by a collision in both types of devices can be calculated as:

$$Pbc_{L_{wo},k,l} = 1 - \frac{f_{L,k}}{1-\tau_{s,k}} - Pbs_{L_{wo},k,l} \tag{60}$$

$$Pbc_{N_{wo},k,l} = 1 - \frac{f_{N,k}}{1-\tau_{b,k}} - Pbs_{N_{wo},k,l} \tag{61}$$

where $l \leq k$, as before.

Similarly, the probability of the backoff countdown being suspended due to successful transmission, if NGV devices employ fallback, is

$$Pbs_{L_w,k,l} = \left(\sum_{i=l}^{3} \frac{n_{L,i}\tau_{s,i}}{(1-\tau_{s,i})(1-\tau_{s,k})} + \sum_{i=l}^{3} \frac{n_{N,i}\tau_{b,i}}{(1-\tau_{b,i})(1-\tau_{s,k})} \right) \cdot \prod_{u=l}^{3} (1-\tau_{s,u})^{n_{L,u}} \prod_{u=l}^{3} (1-\tau_{b,u})^{n_{N,u}} - \frac{\tau_{s,k}}{(1-\tau_{s,k})^2} \prod_{u=l}^{3} (1-\tau_{s,u})^{n_{L,u}} \prod_{u=l}^{3} (1-\tau_{b,u})^{n_{N,u}} \tag{62}$$

for legacy devices, and

$$\begin{aligned} Pbs_{N_w,k,l} = {} & \left(\sum_{i=l}^{3} \frac{n_{L,i}\tau_{s,i}}{(1-\tau_{s,i})(1-\tau_{b,k})} \prod_{u=l}^{3} (1-\tau_{s,u})^{n_{L,u}} - \frac{\tau_{b,k}}{(1-\tau_{b,k})^2} \prod_{u=l}^{3} (1-\tau_{s,u})^{n_{L,u}} \right) \\ & + P_{b,k} \left(\sum_{i=l}^{3} \frac{n_{N,i}\tau_{b,i}}{(1-\tau_{b,i})(1-\tau_{b,k})} \prod_{u=l}^{3} (1-\tau_{b,u})^{n_{N,u}} - \frac{\tau_{b,k}}{(1-\tau_{b,k})^2} \prod_{u=l}^{3} (1-\tau_{b,u})^{n_{N,u}} \right) \\ & + Q_{p,k} \left(\sum_{i=l}^{3} \frac{n_{N,i}\tau_{p,i}}{(1-\tau_{p,i})(1-\tau_{p,k})} \prod_{u=l}^{3} (1-\tau_{p,u})^{n_{N,u}} - \frac{\tau_{b,k}}{(1-\tau_{b,k})^2} \prod_{u=l}^{3} (1-\tau_{p,u})^{n_{N,u}} \right) \end{aligned} \tag{63}$$

for NGV devices.

Subsequently, the probability of the backoff counter being interrupted due to a collision for both legacy and NGV devices can be written as

$$\begin{aligned} Pbc_{L_w,k,l} &= 1 - \frac{f_{L,k}}{1-\tau_{s,k}} - Pbs_{L_w,k,l} \\ Pbc_{N_w,k,l} &= 1 - \frac{f_{N,k}}{P_{b,k}(1-\tau_{b,k}) + Q_{p,k}(1-\tau_{p,k})} - Pbs_{N_w,k,l} \end{aligned} \tag{64}$$

where $l \leq k$.

PGF for the non-zero value of the backoff counter in the vertical transfer in no fallback case is

$$Bfl_{X,k}(z) = \frac{\frac{f_{X,k}}{1-\tau_{X,k}} z Bfnl_{X,k}(z)}{1 - z(Pbs_{X,k,k}Sw_{X,k}(z) + Pbc_{X,k,k}Ct_{X,k})} \tag{65}$$

while the corresponding PGFs when NGV devices use fallback are

$$\begin{aligned} Bfl_{L_w,k}(z) &= \frac{\frac{f_{L,k}}{1-\tau_{s,k}} z Bfnl_{X,k}(z)}{1 - z(Pbs_{L_w,k,k}Sw_{L_w,k}(z) + Pbc_{L_w,k,k}Ct_{L_w,k})} \\ Bfl_{N_w,k}(z) &= \frac{\frac{f_{N,k}}{P_{b,k}(1-\tau_{b,k}) + Q_{p,k}(1-\tau_{p,k})} z Bfnl_{X,k}(z)}{1 - z(Pbs_{N_w,k,k}Sw_{N_w,k}(z) + Pbc_{N_w,k,k}Ct_{N_w,k})} \end{aligned} \tag{66}$$

Likewise, PGFs for lateral transfer, connecting backoff arbitration blocks, can be written as

$$Bfs_{X,0}(z) = g_{X,0}z + (Pbs_{X,0,0}Sw_{X,0}(z)$$

$$+ Pbc_{X,0,0}Ct_{X,0}(z))Bfl_{X,0}(z)$$

$$Bfs_{X,1}(z) = g_{X,1}z + \Big[(1-f_{X,1})^{A_{X,1,max}}(Pbs_{X,1,1} Sw_{X,1}(z) + Pbc_{X,1,1}Ct_{X,1}(z)) + f_{X,1}^{A_{X,1,max}} \cdot (Pbs_{X,1,0}Sw_{X,0}(z) + Pbc_{X,1,0}Ct_{X,0}(z))\Big] Bfl_{X,1}(z)$$

$$Bfs_{X,2}(z) = g_{X,2}z + \Big\{(1-f_{X,2}^{A_{X,2,max}})(Pbs_{X,2,2}Sw_{X,2}(z) + Pbc_{X,2,2}Ct_{X,2}(z)) + f_{X,2}^{A_{X,2,max}} \Big[(1-f_{X,1}^{A_{X,1,max}})(Pbs_{X,2,1}Sw_{X,1}(z) + Pbc_{X,2,1} Ct_{X,1}(z)) + f_{X,1}^{A_{X,1,max}}(Pbs_{X,2,0}Sw_{X,0}(z) + Pbc_{X,2,0}Ct_{X,0}(z))\Big]\Big\} Bfl_{X,2}(z)$$

$$Bfs_{X,3}(z) = g_{X,3}z + \{(1-f_{X,3}^{A_{X,3,max}})(Pbs_{X,3,3}Sw_{X,3}(z) + Pbc_{X,3,3}Ct_{X,3}(z)) + f_{X,3}^{A_{X,3,max}}[(1-f_{X,2}^{A_{X,2,max}}) (Pbs_{X,3,2}Sw_{X,2}(z) + Pbc_{X,3,2}Ct_{X,2}(z)) + f_{X,2}^{A_{X,2,max}}((1-f_{X,1}^{A_{X,1,max}}) (Pbs_{X,3,1}Sw_{X,1}(z) + Pbc_{X,3,1}Ct_{X,1}(z)) + f_{X,1}^{A_{X,1,max}}(Pbs_{X,3,0}Sw_{X,0}(z) + Pbc_{X,3,0}Ct_{X,0}(z)))]\} Bfl_{X,3}(z) \quad (67)$$

PGF for the duration of backoff phase i for traffic class k of both legacy and NGV devices on the medium can be written as

$$B_{X,k,i}(z) = \frac{Bfnl_{X,k}(z)}{W_{X,k,i}} + \frac{Bfl_{X,k}(z)}{W_{X,k,i}} \sum_{l=1}^{W_{X,k,i}-1} Bfs_{X,k}(z)^l \quad (68)$$

PGF for the total backoff time, considering all backoff phases except the zeroth phase, with an extended retry limit $R > m_{X,k}$ can be written as:

$$\begin{aligned} &Bof_{X,k}(z) \\ &= \sum_{i=1}^{m_{X,k}+1} \prod_{j=0}^{i-1} B_{X,k,j}(z)(1-\delta_{Y,k}\gamma_{X,k})^{i-1} \\ &\cdot Ct_{X,k}(z)^{i-1}\delta_{Y,k}\gamma_{X,k} + \sum_{i=m_{X,k}+1}^{R} \prod_{j=0}^{m_k} B_{X,k,j}(z) \\ &\cdot B_{X,k,m_k}(z)^{i-m_{X,k}}(1-\delta_{Y,k}\gamma_{X,k})^i Ct_{X,k}(z)^i\delta_{Y,k}\gamma_{X,k} \\ &+ \prod_{j=0}^{m_{X,k}} B_{X,k,j}(z)B_{X,k,m_{X,k}}(z)^{R-m_{X,k}} \\ &\cdot (1-\delta_{Y,k}\gamma_{X,k})^{R+1}Ct_{X,k}(z)^{R+1} \end{aligned} \quad (69)$$

The initial two moments of this distribution are $Bof^{(1)}_{X,k}(z) = Bof'_{X,k}(1)$ and $Bof^{(2)}_{X,k}(z) = Bof''_{X,k}(1) + Bof'_{X,k}(1)$, respectively.

By the same token, PGF for the duration of the backoff process can be expressed as

$$Bzof_{X,k}(z) = \delta_{Y,k}\gamma_{X,k} + e^{-s(rts+cts+AIFS_{X,k}+sifs)}$$

$$\begin{aligned} &+ \sum_{i=2}^{m_{X,k}+1} \prod_{j=0}^{i-1} B_{X,k,j}(z)(1-\delta_{Y,k}\gamma_{X,k})^{i-1} \\ &\cdot Ct_{X,k}(z)^{i-1}\delta_{Y,k}\gamma_{X,k} + \sum_{i=m_{X,k}+1}^{R} \prod_{j=0}^{m_{X,k}} B_{X,k,j}(z) \\ &\cdot B_{X,k,m_{X,k}}(z)^{i-m_{X,k}} \\ &(1-\delta_{Y,k}\gamma_{X,k})^i Ct_{X,k}(z)^i\delta_{Y,k}\gamma_{X,k} \\ &+ \prod_{j=0}^{m_{X,k}} B_{X,k,j}(z)B_{X,k,m_{X,k}}(z)^{R-m_{X,k}} \\ &\cdot (1-\delta_{Y,k}\gamma_{X,k})^{R+1}Ct_{X,k}(z)^{R+1} \end{aligned} \quad (70)$$

REFERENCES

[1] F. Abdolahi, J. Mišić, and V. B. Mišić, "Performance of IEEE 802.11bd channel bonding with fallback," in *Proc. GLOBECOM IEEE Global Commun. Conf.*, Dec. 2023, pp. 1956–1961.
[2] F. Abdolahi, J. Mišić, and V. B. Mišić, "Performance of IEEE802.11bd for legacy and NGV devices with channel bonding and no fallback," in *Proc. 19th Int. Conf. Wireless Mobile Comput., Netw. Commun. (WiMob)*, Jun. 2023, pp. 356–361.
[3] J. Ahn, Y. Kim, and R. Kim, "A novel WLAN vehicle-to-anything (V2X) channel access scheme for IEEE 802.11p-based next-generation connected car networks," *Appl. Sci.*, vol. 8, no. 11, p. 2112, Nov. 2018.
[4] W. Ahn and R. Y. Kim, "Distributed triggered access for BSM dissemination in 802.11bd V2V networks," *Appl. Sci.*, vol. 10, no. 1, p. 311, Dec. 2019.
[5] W. Anwar, N. Franchi, and G. Fettweis, "Physical layer evaluation of V2X communications technologies: 5G NR-V2X, LTE-V2X, IEEE 802.11bd, and IEEE 802.11p," in *Proc. IEEE 90th Veh. Technol. Conf. (VTC-Fall)*, Sep. 2019, pp. 1–7.
[6] F. Arena, G. Pau, and A. Severino, "A review on IEEE 802.11p for intelligent transportation systems," *J. Sensor Actuator Netw.*, vol. 9, no. 2, p. 22, 2020.
[7] A. Belogaev, A. Elokhin, A. Krasilov, E. Khorov, and I. F. Akyildiz, "Cost-effective V2X task offloading in MEC-assisted intelligent transportation systems," *IEEE Access*, vol. 8, pp. 169010–169023, 2020.
[8] S. Ehsanfar, K. Moessner, A. K. Gizzini, and M. Chafii, "Performance comparison of IEEE 802.11p, 802.11bd-draft and a unique-word-based PHY in doubly-dispersive channels," in *Proc. IEEE Wireless Commun. Netw. Conf. (WCNC)*, Apr. 2022, pp. 1815–1820.
[9] V. P. Harigovindan, A. V. Babu, and L. Jacob, "Tuning transmission opportunity (TXOP) limits for providing bit-based fairness in IEEE 802.11p V2I networks," in *Proc. Int. Conf. Adv. Comput., Commun. Informat.*, Aug. 2012, pp. 248–254.
[10] H. Hong, Y. Y. Kim, R. Y. Kim, and W. Ahn, "An effective wide-bandwidth channel access in next-generation WLAN-based V2X communications," *Appl. Sci.*, vol. 10, no. 1, p. 222, Dec. 2019.
[11] M. Iqbal, C. Rochman, V. Sathya, and M. Ghosh, "Impact of changing energy detection thresholds on fair coexistence of Wi-Fi and LTE in the unlicensed spectrum," in *Proc. Wireless Telecommun. Symp. (WTS)*, Apr. 2017, pp. 1–9.
[12] J. Saranya, M. H. Reddy, and V. P. Harigovindan, "Improving aggregate utility and fairness in multi-lane vehicle-to-infrastructure networks," in *Proc. Int. Conf. Inf. Sci. (ICIS)*, Aug. 2016, pp. 252–257.
[13] R. Jacob, W. Anwar, N. Schwarzenberg, N. Franchi, and G. Fettweis, "System-level performance comparison of IEEE 802.11p and 802.11bd draft in highway scenarios," in *Proc. 27th Int. Conf. Telecommun. (ICT)*, Oct. 2020, pp. 1–6.
[14] B. Ji, X. Zhang, S. Mumtaz, C. Han, C. Li, H. Wen, and D. Wang, "Survey on the Internet of vehicles: Network architectures and applications," *IEEE Commun. Standards Mag.*, vol. 4, no. 1, pp. 34–41, Mar. 2020.
[15] J. B. Kenney, "Dedicated short-range communications (DSRC) standards in the United States," *Proc. IEEE*, vol. 99, no. 7, pp. 1162–1182, Jul. 2011.
[16] M. Mehrnoush, S. Roy, V. Sathya, and M. Ghosh, "On the fairness of Wi-Fi and LTE-LAA coexistence," *IEEE Trans. Cognit. Commun. Netw.*, vol. 4, no. 4, pp. 735–748, Dec. 2018.

[17] Y. L. Morgan, "Notes on DSRC & WAVE standards suite: Its architecture, design, and characteristics," *IEEE Commun. Surveys Tuts.*, vol. 12, no. 4, pp. 504–518, 4th Quart., 2010.
[18] G. Naik, B. Choudhury, and J.-M. Park, "IEEE 802.11bd & 5G NR V2X: Evolution of radio access technologies for V2X communications," *IEEE Access*, vol. 7, pp. 70169–70184, 2019.
[19] R. Oliveira, C. Montez, A. Boukerche, and M. S. Wangham, "Reliable data dissemination protocol for VANET traffic safety applications," *Ad Hoc Netw.*, vol. 63, pp. 30–44, Aug. 2017.
[20] V. P. Harigovindan, A. V. Babu, and L. Jacob, "Fairness assurance through TXOP tuning in IEEE 802.11p vehicle-to-infrastructure networks for drive-thru internet applications," *Commun. Netw.*, vol. 5, no. 1, pp. 69–83, 2013.
[21] F. Pereñiguez, J. Santa Lozano, P. J. Fernández, F. Bernal, A. F. Skarmeta, and T. Ernst, "The use of IPv6 in cooperative ITS: Standardization viewpoint," in *Vehicular ad hoc Networks: Standards, Solutions and Research*, C. Campolo, A. Molinaro, and R. Scopigno, Eds. Cham, Switzerland: Springer, 2015, pp. 253–282.
[22] S. Rashwand and J. Mišic, "IEEE 802.11e EDCA under bursty traffic—How much TXOP can improve performance," *IEEE Trans. Veh. Technol.*, vol. 60, no. 3, pp. 1099–1115, Mar. 2011.
[23] M. A. Togou and G.-M. Muntean, "A dynamic transmission opportunity allocation scheme to improve service quality of vehicle-to-vehicle non-safety applications," in *Proc. IEEE 87th Veh. Technol. Conf. (VTC Spring)*, Jun. 2018, pp. 1–5.
[24] V. Torgunakov, V. Loginov, and E. Khorov, "A study of the impact of the contention window on the performance of IEEE 802.11bd networks with channel bonding," in *Proc. Int. Conf. Eng. Telecommun. (EnT)*, Nov. 2021, pp. 1–5.
[25] V. Torgunakov, V. Loginov, and E. Khorov, "A study of channel bonding in IEEE 802.11bd networks," *IEEE Access*, vol. 10, pp. 25514–25533, 2022.
[26] V. A. Torgunakov, V. A. Loginov, E. M. Khorov, and A. I. Lyakhov, "Algorithm for adaptative selection of a contention window in IEEE 802.11bd networks," *J. Commun. Technol. Electron.*, vol. 67, no. S2, pp. S241–S247, Dec. 2022.
[27] A. Triwinarko, "Cross-Layer design for vehicular ad-hoc networks (VANETs)," Ph.D. thesis, Institut d'Electronique de Micróelectronique et de Nanotechnologie, Ḍepartement Opto-Acousto- Electronique, Hauts-de-France, Valenciennes, France, 2021.
[28] E. T. Whittaker and G. N. Watson, *A Course of Modern Analysis: An Introduction to the General Theory of Infinite Processes and of Analytic Functions; With an Account of the Principal Transcendental Functions*. Cambridge, U.K.: Cambridge Univ. Press, 1920.
[29] B. Y. Yacheur, T. Ahmed, and M. Mosbah, "Analysis and comparison of IEEE 802.11p and IEEE 802.11bd," in *Communication Technologies for Vehicles*, F. Krief, H. Aniss, L. Mendiboure, S. Chaumette, and M. Berbineau, Eds. Cham, Switzerland: Springer, 2020, pp. 55–65.
[30] K. Zheng, Q. Zheng, H. Yang, L. Zhao, L. Hou, and P. Chatzimisios, "Reliable and efficient autonomous driving: The need for heterogeneous vehicular networks," *IEEE Commun. Mag.*, vol. 53, no. 12, pp. 72–79, Dec. 2015.

FARZANEH ABDOLAHI (Graduate Student Member, IEEE) is currently pursuing the Ph.D. degree in computer science with Toronto Metropolitan University (formerly Ryerson), Toronto, Ontario, Canada. Her research interests include performance evaluation of wireless networks, cloud computing, and exploring emerging research avenues within vehicular networks.

JELENA MIŠIĆ (Fellow, IEEE) is currently a Professor of computer science with Toronto Metropolitan University (formerly Ryerson), Toronto, Ontario, Canada. She has published four books, more than 165 articles in archival journals and about 220 papers at international conferences in the areas of computer networks and security. She serves on the Editorial Boards for IEEE TRANSACTIONS ON VEHICULAR TECHNOLOGY, IEEE IoT JOURNAL, IEEE NETWORK, *Computer Networks*, and *Ad Hoc Networks*. She is a member of ACM.

VOJISLAV B. MIŠIĆ (Senior Member, IEEE) is currently a Professor of computer science with Toronto Metropolitan University (formerly Ryerson), Toronto, Ontario, Canada. His research interests include performance evaluation of wireless networks and blockchain technology. He serves on the Editorial Boards for IEEE TRANSACTIONS ON NETWORK SCIENCE AND ENGINEERING and *Peer-to-Peer Networks and Applications*.